TÉCNICO LISBOA

Planar Antennas for Wireless Power Transfer at mm-Waves

Francisco Filipe Silva Lopes da Ressurreição Martins

Thesis to obtain the Master of Science Degree in

Electrical and Computers Engineering

Supervisor(s): Prof. Carlos António Cardoso Fernandes
Prof. Sérgio de Almeida Matos

Examination Committee

Chairperson: Professor José Eduardo Charters Ribeiro da Cunha Sanguino
Supervisor: Professor Carlos António Cardoso Fernandes
Members of Committee: Professor Marco Alexandre dos Santos Ribeiro

November 2022

Declaration: I declare that this document is an original work of my own authorship and that it fulfills all the requirements of the Code of Conduct and Good Practices of the Universidade de Lisboa.

Declaração: Declaro que o presente documento é um trabalho original da minha autoria e que cumpre todos os requisitos do Código de Conduta e Boas Práticas da Universidade de Lisboa.

Acknowledgments

I would like to thank Instituto de Telecomunicações for all the supporting material available that allowed me to fulfil the concretization of this work. To my supervisors, Professor Carlos Fernandes and Professor Sérgio Matos for guiding me through the right directions and giving me the support to complete this journey. To Mr. Carlos Brito, for all the hard work building the needed circuits, in such a short time, and with all the adversities that he had to deal with. A special mention to João Felício, for all the hard work and availability to help me succeed with this thesis. For all the helping process of creation, fabrication and measuring.

To my colleagues Carlos Loureiro and Artur Alves, for helping me in moments where I felt lost and for proving me that a college degree is not supposed to be made by our own, but always with the help of each other, thank you for everything.

To all my colleagues and friends that I have met over the past few years during my journey in Instituto Superior Técnico. I will keep all the memories, all the laughs and cries, all the support and friendship that I received from you. Thank you for those wonderful times.

I am especially grateful for my family and all the support and encouragement they gave me along this path. I would like to thank my parents, Rui Martins and Telma Lopes, for not giving up on motivating me, even when I felt I was not good enough. Endless nights when I felt one-step away from giving up, your warming love and dedication always proved to be enough to go through another day, through another battle, through another obstacle. Your love is unmeasurable. Also, my sisters, Clara Martins and Margarida Martins, and the brother that life gave me, Adriano Alves, thank you for being always beside me, and for helping me forgetting the bad moments and look at the future in a hopeful way.

Finally, but not least, I would especially like to thank to my girlfriend, Inês Caetano. I cannot describe how important is your presence in my life. For supporting me when I was down, when I felt hopeless, when I needed a conscious voice to help me focusing on the important things. Thank you for all your love and for being my best friend.

And to everyone that, directly or indirectly, influenced me and made me the man that I am today, to all my honest and deepest thank you.

Abstract

With the demand for better, smaller and cheapest satellites to use for space mission purposes, Cubesats, satellites of small dimensions that allow to be launched in a higher quantity with low production costs, are establishing as one of the most prolific satellites to consider. More specifically, with cubesats of 1U and 3U dimensions, it is possible to execute missions with cubesats constellations that make the results achievement quicker and easier.

For missions using cubesats constellations, the storing and transfer of energy from one satellite to another may be a key strategy to guarantee the best performance possible.

The purpose of this thesis is to study the impact on the power transfer efficiency of using Gaussian beams to wirelessly transfer energy from a cubesat to another. Specifically, taking a 3U cubesat, wirelessly transferring power to a smaller cubesat, 1U, at distances within the near-field range. To do so, a system of two opposite reflect arrays antennas (RA), are designed and fabricated to generate the Gaussian beam and focus its energy into a collecting aperture. The used RAs are low-cost planar structures, fabricated with printed circuit technology, populated with 2-square rings unit cells, to achieve the required phase front correction, at 24 GHz.

Each RA uses a horn antenna at its focus, one to illuminate the larger RA with energy, and the other to receive the energy collected by the smaller RA. This strategy, together with the use of the Gaussian beam ensure a significant reduction of wasted energy by “spill-over”, compared to simple wave propagation between two antennas.

Keywords: satellites, CubeSats, wirelessly transfer power, antennas, reflect arrays, k_a band, phoenix cells, directivity.

Resumo

Com o aumento da procura por melhores satélites, mais pequeno e mais baratos para serem usados em missões espaciais, os CubeSats, satélites de pequenas dimensões que permitem que sejam lançados em maior quantidade por um custo de produção mais baixo, têm se afirmado como um dos satélites mais prolíferos e rentáveis a serem considerados. Mais especificamente, através do uso de CubeSats de dimensões 1U e 3U, é possível executar missões recorrendo a constelações de CubeSats, permitindo a obtenção de resultados de forma mais rápida e eficaz.

Para missões espaciais que usam constelações de cubesats, o armazenamento e transferência de energia de um satélite para outro pode ser uma estratégia fulcral para garantir o melhor desempenho possível.

O objetivo desta dissertação passa por estudar o impacto que o uso de feixes Gaussianos poderá ter no que toca à eficiência da transferência de energia sem fios de um cubesat para outro. Mais especificamente considerando um cubesat de dimensão 3U e transferir energia sem fios para um cubesat de dimensões menores, 1U, funcionando em distâncias que estão dentro da zona de near-field. Para isso, um sistema com duas antenas reflectarray (RA) opostas é desenhado e fabricado de modo a gerar um feixe Gaussiano e focar a sua energia numa abertura colectora. Os RAs usados são estruturas planas de baixo custo, fabricadas com tecnologia de impressão de circuitos, e populadas com células unitárias constituídas por 2 anéis quadrados, de modo a atingir a correção de fase da frente de onda necessária, a 24 GHz.

Cada RA utiliza uma corneta no seu ponto focal, uma para iluminar o RA maior com energia e o outro para receber a energia colectada pelo RA mais pequeno. Esta estratégia, em conjunto com o uso de feixe Gaussiano, permite assegurar uma redução significativa da energia desperdiçada por “spill-over”, em contraste com a propagação de ondas simples entre duas antenas.

Palavras-chave: satélites, CubeSats, transferir energia sem fios, antenas, reflectarrays, banda k_a, diretividade

Contents

List of figures

Acronyms

1U One Unit

3U three Units

CubeSat Cube Satellite

CST_MWS CST Microwave Studio

DSN Deep Space Network

EO Earth Observations

GEO Geostationary Earth Orbit

IGY International Geophysical Year

LEO Low Earth Orbit

RA Reflect Array

SSPS Space Solar Power Systems

TA Transmit Array

UV Ultra Violet

WPT Wireless Power Transfer

1. Motivation and objectives

For many satellites missions, one of the biggest issues is the durability of their energy. It is not endless, nor can be continuously restored throughout the mission.

One of the possible solutions is to implement on the satellites solar panels that can absorb sun energy and turn it into electrical energy, capable to sustain the functionalities of the satellite. Whit this, however, comes another issue: the size of the satellites. For bigger satellites, this can be a main solution, but for smaller satellites, like the CubeSats, it does not solve the problem since, due to their size, they cannot support big solar panels, which means they cannot absorb enough quantity of solar light to restore their energy. They must have deployable panels, so it does not affect their performance nor their launch to space.

One factor that can represent a solution for this problem is that, for most of the situations, these small satellites operate in “constellations”, meaning they are launched into space in a certain number and work as a team, covering a large area. If there are different sizes of satellites, it may be viable to use some of them, of bigger size, to receive the Sun energy and share it with other smaller satellites, through antennas manufactured specifically for that purpose.

This solution must be, obviously, wireless, and it needs to be able to operate for short distances, since the satellites will not be too much far from each other. On the other hand, the way the power is transmitted must avoid at the maximum the amount of energy that is wasted by “spill-over”. The result is a fully working constellation of small satellites that can cover a considerable area of space, that can fulfil their missions, from gathering space particles for study, studying the weather or even for telecommunication purposes.

The main goal of this work is then to study if reflect array antennas, configured to produce Gaussian beams, will wirelessly transfer power, from one Cubesat to another, focusing the maximum intensity possible on the desired collecting surface area, with the best energy transfer efficiency possible. Reflect-arrays are planar, foldable to compact volume, and have low mass; therefore, they are a natural choice for use in cubesats. In fact, due to the CubeSats sizes, the antennas are limited in area and mass: while for the 1U CubeSat, the smallest one, the RA can have a maximum area of 10x10 cm, in the case of the 3U the area will be 30x30 cm, and it has to be folded for launch. This RA’s area difference has also an impact on the process of studying and fabricating each RA prototype. Since the cubesats are nanosatellites, with a mass between 1 kg to 10 kg, the RAs must be flat, not only to reduce the total area of the cubesat but to avoid increasing as much as possible its maximum mass. Furthermore, the distance between the two satellites also has an impact, since it affects the intensity the beam leaves one reflect array and focuses on the other one.

The appropriate operation frequency for Wireless Power Transfer must be chosen as a compromise between the size of the transmitting, and collecting antenna surfaces, the focusing distance, and the RF-DC conversion efficiency. The 24 GHz frequency was established as this compromise.

In the end, and after considering all the conditions and restrictions mentioned above, the desired efficiency is the main goal to be kept in mind: for a ratio D_{Rx}/w_0 close to one, being D_{Rx} the size of the transmitting reflect-array and w_0 the minimum waist of the Gaussian beam, the transfer efficiency should achieve relatively high values, over 80%. However, the system has inherent losses, associated with energy spill over past the edges of the reflect-arrays and respective feeds, and reflection efficiency of the reflect-array unit cells. The objective of this thesis is to fully characterize the proposed WPT system by simulation and the experimental prototype.

2. State of the Art

2.1. Small Satellites and CubeSats

During the cold war, both United States of America and Soviet Union tried to conquer Space through an enormous effort to launch as many space missions as they could. This led them to really change and develop the whole Satellites world.

During 1957-1958 International Geophysical Year (IGY), what we can call the beginning of Space Age, both countries launched three small satellites: Sputnik I, Explorer I and Vanguard I (Figure 1). The desired size of these satellites was heavily influenced by the period concerned, since both US and Soviet Union were cautious and discreet about the secrecy of their space and nuclear bombs programs. In fact, only Vanguard program (from the U.S. Navy) was conducted completely in the open [1].

The 1960s space programs efforts were mainly dominated by political matters, with the exploration of the Solar System and human space missions, culminating, in 1969, with the Apollo Moon landings. This big effort allowed a rapid evolution to provide civil communications (through voice and television) and Earth Observations (EO) for meteorology, controlled by governments [2].

The appearance of available microelectronic components enabled the construction of even smaller satellites, with smaller teams, since each space mission, concerning the building of the satellite and required advanced and expensive technologies, was a costly, risky and complex program [2].

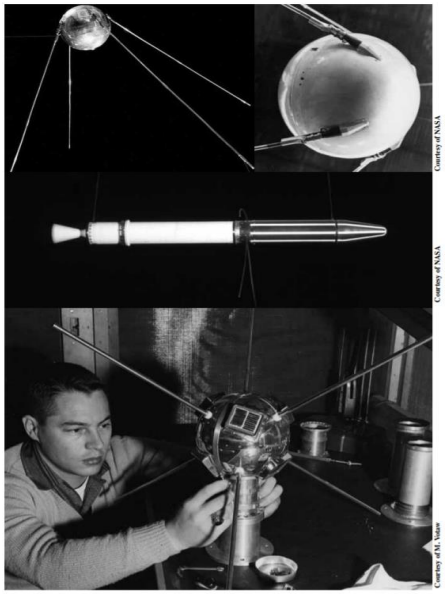

Figure 1 - Perspectives of the Sputnik I (top); Explorer I (middle); Robert Bauman with Vanguard I (bottom) [1].

Between 1964 and 1967, Strela-1 experimental satellites were launched. After that period, in 1986 Soviet Union launched 25 microsatellites (10 to 100-kg mass) as part of a communications constellation. Twenty-four of them were military communications satellites, called *Strela-1M,* with 61-kg mass. There were no nanosatellites nor picosatellites launched that year and during a certain period, as it shown in Figure 2, these spacecrafts were designed to provide medium-range, record-and-forward communications using Low Earth Orbit (LEO). Strela-1M satellites were launched eight at a time, twice a year, on Kosmos-3M boosters, into an approximately 1500-

km altitude orbit at 74˚ inclination. At the time, their operational lifetime was about 2 years and between 1970 and 1993, 360 Strela-1M spacecraft were launched. They were later succeeded by heavier and non-microsatellite class, Strela-2M and Strela-3M communications satellites [3].

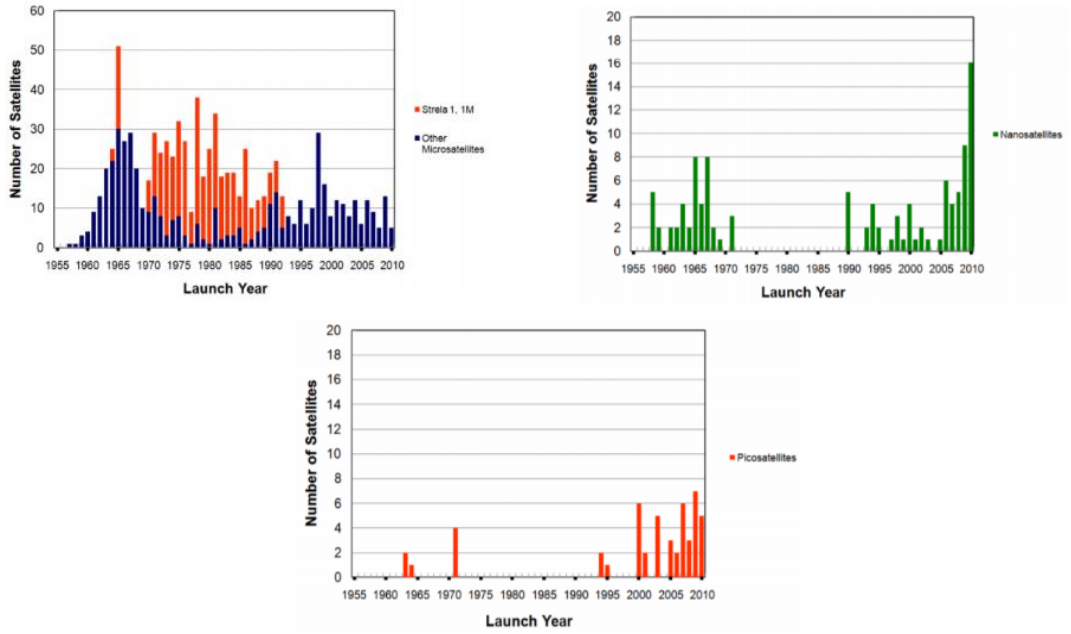

Figure 2 - Number of satellites launched per year from 1955 to 2010: Strela 1, 1M and other microsatellites (top left), nanosatellites (top right) and picosatellites (bottom) [3]

The two small satellites conferences held in 1987, the first one sponsored by the American Institute of Aeronautics and Astronautics (AIAA) and the Defense Advanced Research Agency (DARPA), the second one, in a more academic participation, culminated in January 21, 1990 with the launch of the French SPOT-2 Earth resources satellite by an Ariane-4, along with three 9-kg mass Radio Amateur Satellite Corporation (AMSAT) microsatellites, a 12-kg mass AMSAT microsatellite called “webersat” and two University of Surrey microsatellites. This was the first flight of the Ariane Structure for Auxiliary Payload (ASAP) ring, able to hold up six small satellites (50-kg mass maximum) with 35 x 35 x 60 cm dimensions maximum. Those AMSAT microsatellites, that can be considered nanosatellites with today’s satellites standards, were 23-cm dimension cubes covered with solar cells (maximum output power of 15.7 W).

In the beginning of the year 2000, on January 27, JAWSAT was putted into orbit. It then released the 22-kg optical Calibration Sphere Experiment, the 52-kg Falconsat-1 (U.S. Air Force Academy), the 5-kg ASUsat-1 and the 25-kg mass OPAL (which, later, ejected three picosatellites from Santa Clara University, a 0.23-kg amateur radio picosatellite called Stensat and two 0.3 kg DARPA).

More and more picosatellites and nanosatellites were placed on orbit through that year (previous and next years also - Figure 2), and in June 2000 an important nanosatellite milestone was achieved, when the 6.5-kg mass SNAP-1 (the first nanosatellite to demonstrate orbital manoeuvring, nearby spacecraft imaging and on-orbit GPS position and velocity determination) was launched along with the 50-kg mass Tsinghua-1 microsatellite, this last one with the purpose of serving as a target platform for a satellite inspection mission [3].

This successful mission led Stanford and the California Polytechnic State University at San Luis Obispo to create and establish a completely new program dedicated to CubeSat [3].

Class	Mass (kg)
Large satellite	>1000
Small satellite	500 to 1000
Mini-satellite	100 to 500
Micro-satellite	10 to 100
Nano-satellite	1 to 10
Pico-satellite	0.1 to 1
Femto-satellite	<0.1

Table 1 - Class and mass (in kg) of the different satellites dimensions [2]

2.2. Millimetre Wave Antennas for Space

Regarding the frequency range used on this project (between 20-30 GHz), antennas that operate on this level are much more compact and have higher gain and much lower cost.

When choosing the type of high gain antenna capable of beam steering for a specific project, normally aperture antennas or antenna arrays are the ones considered. Usually aperture antennas are bulkier when compared to antenna arrays, which requires the integration on the mechanic of the craft, highly increasing its weight, cost and time of implementation and launch cost.

In that way, a much lighter and not expensive solution are the antenna arrays.

This sub chapter focuses on different types of those antennas, to provide knowledge about the technology used for this project.

2.2.1. Transmit Arrays

One of the approaches to realize a high gain is based on antenna array theory where interference of elements radiation is controlled.

A transmit array (TA) antenna is described as a set of a flat transmitting surface illuminated by a feed source, located on a focal point. One or multiple layers compose the flat surface, where there is a printed antenna elements array. The basic function of these elements, regarding their transmission coefficients, is to transform from a spherical phase front to a planar phase front, resulting in a high gain radiation beam [4].

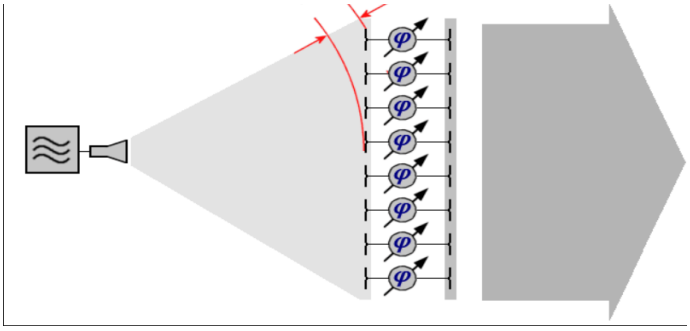

Figure 3 - Transmit Array and phase shift process [38]

The array consists of many small antennas that are responsible for the phase shift and make possible to achieve a high gain. For that reason, they are typically used for high frequency end of the radio spectrum, in microwave bands, in which the antenna elements are small [5]

2.2.2. Reflect Arrays

A reflect array (RA) have similar functionality when compared to a transmit array. It is the combination of reflector antennas and phased array antennas working principles. It has a feed, also located at a focal point, and a planar surface where the unit cells responsible for the phase shift are located. After the phase shift happens, instead of being transmitted as a steering beam, the planar metallic surface will reflect the beam with an angle that depends on the incident angle of the wave.

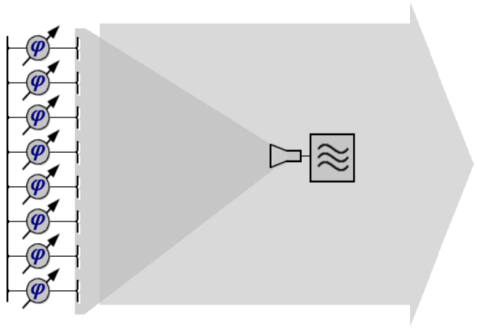

Figure 4 - Reflect Array and phase shift process [38]

For the phase shift process, there's a relation given by

$$-k_0 d + \psi = constant \quad (1)$$

This means that for a distance d from the feed to the planar surface, multiplied by the wavenumber, added to the phase shift introduced by each cell, the relation between all those factors must be constant for every point of the planar surface, so that the phase can shift and it can reflect a planar phase front.

When comparing TA and RA, TA have a more compact form factor. RA antennas are harder to implement, since the feed is behind the surface, and so it is important to take into account the position of the focal point, so that it avoids the shadow area, the zone where the beam is reflected. However, the design and optimization of RA antennas are much easier to work with, instead of the TA antennas.

2.2.3. Unit Cells

Like dielectric lens working principle, in every zone of the RA or the TA, an appropriate phase shift is added to the incident field. This phase shift is provided by individual constant thickness unit cells, which are distributed along the complete planar surface of the TA/RA. This gives a big advantage comparing to lenses, where the phase shift is provided by adjusting its profile, since it requires much less mass and offers more flexibility.

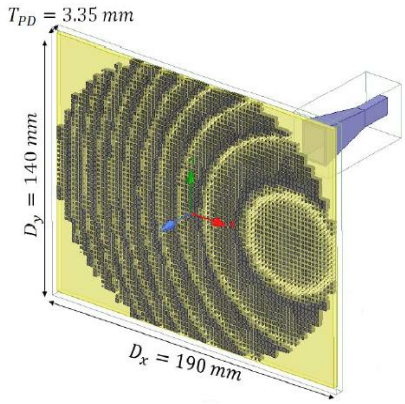

Figure 5 - Constitution of a TA with a feed (horn) and the planar surface filled with unit cells [6]

Despite having constant thickness and the same size, unit cells' design present different phase shift values throughout the planar surface. This unit cells must ensure minimum reflection and insertion loss, as well as a phase range that goes up to 360 degrees to ensure every point of the surface has a phase correction of the incident wave so it can produce continuous phase radiation results [6]. Even considering a certain number of levels in the [0, 360˚] range, enough to obtain those radiation results, and unit cells are designed for infinite periodic surfaces, the reality is that adjacent cells are not equal, the size changes according to the phase distribution. This means that the larger the phase transition between adjacent cells, the larger the phase and reflection loss degradation [7].

The unit cells are made of multiple dielectric layers (Figure 6), with different, that add each one a small phase shift. The bigger the number of layers, the bigger the maximum achievable phase shift range. The larger layers are responsible for the largest cell phase shift, since it reduces with the decrease of the size of the patches [7].

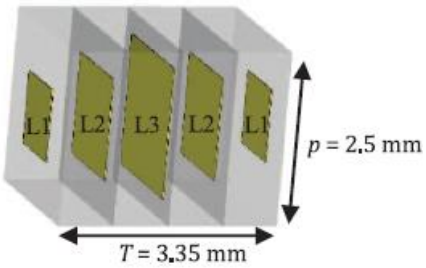

Figure 6 - Cell composition made of five layers [7]

When designing unit cells, there are two different approaches regarding the generation of phase shifts. The first approach means varying the centre frequency of the designed unit cell, which leads to designing a discrete number of cells with very small geometry differences, ensuring that all have good transmission coefficients within a certain frequency band, but providing different phase shifts at that band, "phase delay" (PD) cells. The second approach means rotating a one-unit cell designed with different angles to provide a continuous phase shift up to 360˚, "phase rotation" (PR) cells [6].

2.2.4. Space Related Antennas issues

The complexity of designing an antenna for space purposes leads to deal with more issues related with that environment than if they were designed to work on Earth.

Most of the satellites, including the CubeSats, work in Low Earth Orbit (LEO), which means they orbit at an altitude of 2000 km or less. At this level, specifically between 100 and 1000 km, there can be found Atomic Oxygen, created by the interaction of Ultraviolet (UV) light and oxygen

molecules. This version of oxygen is an issue to consider since it has very corrosive atoms that, with time, affect and damage the spacecraft, and consequently, the antenna.

Another space issues to consider are the Van Allen belts. Discovered during the launch of the Explorer I satellite, in 1958, it has an inner belt that starts at 1000 km above Earth's surface and can reach a minimum altitude of 250 km. In this area, where LEO satellites spend nearly 30% of their time, during a solar flare (like the ones that happen when testing nuclear bombs), the number of protons suddenly increases by more than a million (protons with energies between 10-100 MeV). This new radiation belt, that can last almost 10 years, is responsible for the breakdown of diodes in the command decoder due to the total radiation dose [8].

Temperature variations are also an important phenomenon to consider since satellites construction materials must be trustable to use for much higher temperature variations. Since the incoming radiation from a thermal radiation source (Earth, Sun, etc) heats the satellite in an asymmetric way, with the side facing the radiation source being hotter than the opposite side (the dark side), mechanisms must exist to allow the satellite to compensate the uneven temperature distribution [9]. In addition, with those variations, the materials contract and expand, which can deteriorate the antenna's performance. This implies low thermal expansion materials.

2.3. Wireless Power Transfer

80% of the energy that sustains our lives comes from fossil fuels. This represents a big threat since shortage Earth resources and global warming started to strike and to affect our lives. If this increasingly consumption does not slow down, all the Earth's fossil fuels will be lost in 100-150 years [10].

Nowadays, with such a huge development in technological devices, computers, with up modern technologies that have a big role in our day-by-day lifestyles, there is a need to reduce the number of batteries and electrical wires that connects it all. Furthermore, technologies that can work with wireless communications gives us a much greener communication system [11].

With many new possibilities for new ways to store and use energy, one that stood out was the Wireless Power Transmission/Transfer (WPT). Since there's unlimited Solar energy supply in space, free from weather conditions, it seems that finding an alternative for fossil fuels, taking advantage of the sun, is probably one of the most plausible ways to do it [10].

The concept, conceived by Dr. Peter Glaser in 1973, was to harvest large amounts of solar energy (with satellites in geostationary Earth Orbit (GEO)), transform it in microwave energy and then transmit it to a rectifying antenna (rectenna) array on Earth that would collect and convert the energy into usable direct current power. It is expected that one day this system could supply enough electrical power to Earth and ensure to humanity the continuation of advancement.

After the first studies for space solar power systems (SSPS) started between 1976 and 1980, where large-scale power infrastructure in space consisting of 60 SSPS were crafted, during the 1980s and 1990s international interest emerged, with Japan being the country with the biggest effort to successfully complete space missions based on this system. NASA also started to put a big effort on this study after 1995, undertaking a new study of the challenges of large-scale SSPS systems. From the early 2000s until today, many articles have been written regarding the study of SSPS systems [12].

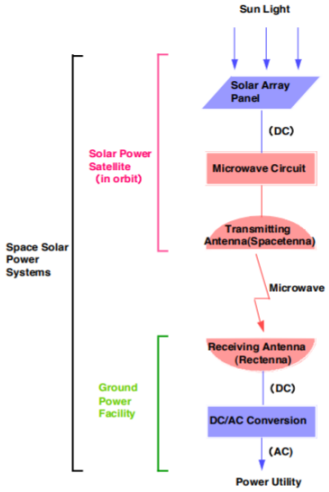

Figure 7 - Space Solar Power Systems [10]

WPT has been an active topic of research, and, since then, many WPT schemes have been implemented in near-field (coupling) and far-field (radiation) regimes. As mentioned before, it can deliver power without wiring infrastructures.

However, the big challenge has been to achieve high efficiency systems at reasonable transfer distances. Although these systems are safe in terms of exposure for humans, and even though they are highly efficient at short distances, the usual WPT schemes require the receiving device to be near the power source. On the other hand, power transfer can be accomplished using short wavelength radio frequency (RF) power radiated from a source aperture to a receive antenna/aperture [13], [14].

Different hypothesis and studies have been performed to try getting better efficiency results. Those studies took into account for the approaches the type of antennas used, the method (a single lens or two lenses), as well as the type of beam or the basic parameters, such as frequency and transmitting distances.

Reference	Frequency	Transmitting distance	Antenna type	Beam Type	Obtained Efficiency	Study Procedures
[13]	77 GHz	5 m	Fresnel antenna	Gaussian Beam	10%-12% of end-to-end efficiency (threshold of 15%)	Theoretical
[15]	5.8 GHz (ISM)	0.4 m	8x8 and 4x4 array antennas, with low-loss 1.524-mm-thick Rogers 4003 substrat	Gaussian Beam	33.2%	Theoretical and Experimental
[16]	2.5 GHz	Between 2.25λ-3.75λ	2 appertures of the same radius placed onto parallel and infinite ground planes	Bessel-Gauss (BGB), Bessel (BB) and TEM	Best efficiency for BGB above 90% when redefining the frequency to 2.565 GHz	Theoretical
[11]	24 GHz	-	Rectifying antenna, with a diode MADS-001317-1320AG	Gaussian Beam	54.2% RF-DC convertion efficiency at 130 mW and 43.6% at 500 mW	Theoretical and experimental
[17]	799-938 GHz	0.136 m	Horn-to-horn power transition	Gaussian Beam	60%	Theoretical and Experimental
[18]	5.8 GHz	5 m	Double-reflector system	Gaussian Beam	63.75%	Theoretical and Experimental
[19]	24 GHz	2 m	Circular horn antennas and a dielectric lens	Gaussian Beam	4.119%	Theoretical and Experimental

Table 2 - Overview on the studies made for Wireless Power Transmission efficiency

Usually, space missions operate from either an on board nuclear power source or using on board solar power generation panels. In both ways, the available power and its utilization rate are limited, which can be a handicap for longer time missions [12].

A new approach, using space solar power (SSP) satellites to provide power to other spacecrafts, taking advantage of the unlimited solar energy source started to emerge [12].

When transferring this system to be conceded for space missions, there are some factors to consider, since the idea is to transfer energy from one satellite to another. This implies the consideration of the working frequency, compromised between antenna size and atmospheric attenuation, the material used to build the spacecraft, beam pointing energy to transmit the microwave power beam precisely to the receiving site and power efficiency, among others [10].

For small satellites, like CubeSats, one possibility came evident. Since those satellites can have missions with other spacecrafts, one of the possible ways to ensure that the satellites energy will not deteriorate is to use the SSPS system, as said before, to transfer energy from one satellite to another.

2.4. Space Applications

Satellites or spacecrafts with integrated antennas are by far the most diverse part of spacecraft technology. They may vary, for example, with frequency or coverage, but the main aspects to be considered are the size, weight and power, according to the satellite launch capabilities. Space communications require high gain antennas, but this requirement is directly proportional to the aperture size, which means that large size antenna technology is a mandatory subject for the purpose [20].

There are four options in terms of types of antennas to be used for space applications: reflectors, lenses, arrays, and hybrids [21]. As we've seen, RA are similar to parabolic reflectors, with the difference that while parabolic reflectors have a curved surface and are bulkier, RA surface is planar, besides having lower mass and production costs. Therefore, RAs, and TAs, are the best choice for space applications.

One of the many space applications that RAs have is for space communication systems, where antennas are typically required to provide multiband operating frequencies. One of the examples of it is the downlink and uplink Ka-bands at 31.8-32.3 GHz and 34.2-34.7 GHz, respectively, for NASA Deep Space Network (DSN). Even though the antenna can cover the bandwidth of the entire frequency range for some cases, multi-band RA designs have been developed to achieve both single and multi-band performances from microwave frequencies up to the THz range [20].

Another possible application for the use of RA antennas is meteorology purposes, like cloud and precipitation monitoring or hurricanes control [22], since the use of high-gain antennas is desirable to have a good sensitivity and resolution for imaging different areas of the Earth's surface. It also helps mitigate the atmosphere attenuation on the system performance, increasing its operational frequency.

TAs are also a good choice for space applications, with many similarities with the RAs, mostly in terms of size, working process and high gain capability.

Due to an increasing demand for high data rate links, for broadband satellite communication (Satcom) systems, TAs operational frequencies at K/Ka band allows them to address higher channel capacities for a large range of purposes. When establishing Satcom on moving links, a planar and very light design for phased array systems is a requirement [23].

In satellite communications, two different frequency bands are required in order to realize the uplink and downlink, which obligates the use of two different types of antennas. This implies the

need for a larger needed space, being the double compared with systems where only one antenna is required. With the use of TA antennas, even though hard to achieve, it is possible to reduce this space utility issue, operating in a dual-band system [24].

The use of RAs and TAs implemented on CubeSats stands as one of the best solutions for space applications, since both have a planar geometry that can be built-in the cubesat faces, saving space and development complexity. Moreover, they can, then, be deployed, which facilitates eventual satellites inter-communications.

One of the applications of RAs for CubeSats was used for MarCo mission. The MarCo mission is proposed to fly alongside the InSight mission to Mars, enabling the transmission of all the collected data to Earth. The spacecraft is a 6U CubeSat which supports a variety of systems, from UHF telecom to power, battery and propulsion systems, and consume almost all the available volume. In order to take advantage of the usable space, and still be able to achieve the gain at the required frequency (28.0 dB at 8.425 GHz), the antenna is comprised of reflect array panels, that deploy perpendicular to the side face [25].

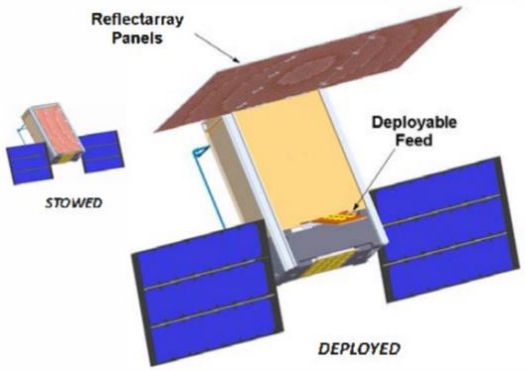

Figure 8 - MarCo CubeSat mission with the deployed reflect array panels [25]

NASA's engineers in the ISARA CubeSat also took advantage of the deployable panels for CubeSats and installed a reflect array on the backside of the panels. Thanks to this system, ISARA provided high gain Ka-band antenna, enabling high bandwidth CubeSat communications, with low mass increase, as well as volume and cost [26].

TAs also stands as a good solution for CubeSats, with similar design as RAs, working on top of the solar panels, in a deployable form. Since focal distance is also an important detail to have in consideration for CubeSats, methods to decrease the focal distance between the feed and the TA surface such as leaky wave feeds [27] or creating virtual intermediary focal points [7] have been researched.

3. Basic concepts and physical principles

3.1. Gaussian Beam

A Gaussian Beam can be described as a beam, usually a laser beam, which electrical field profile in a plane perpendicular to the beam axis is given by a Gaussian function.

The evolution, through space, of the beam's intensity, is described as

$$I(r,z) = \frac{P}{\pi w(z)^2/2} e^{\left(\frac{-2r^2}{w(z)^2}\right)} \quad (2)$$

Where r is the radial distance away from the axis, w(z) is the radius of the laser beam where the irradiance is $1/e^2$ (13.5%) of the maximum value, z is the distance propagated from the plane where the wave front is flat and P is the total power of the beam.

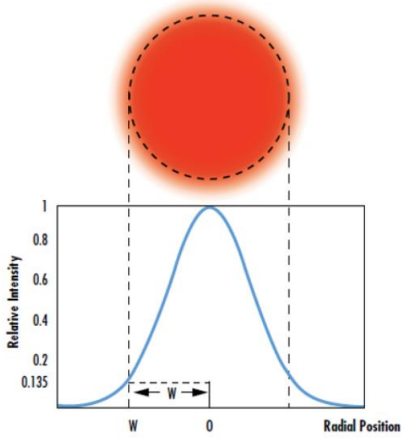

Figure 9 - Gaussian beam intensity [28]

The fact that in the centre of the beam the intensity is at its highest does not mean that it will remain always with approximately the same values.

Due to diffraction, the Gaussian beam converges and diverges from what is called the minimum beam waist w_0, where the beam diameter reaches its minimum.

Assuming that the electric field is focused from the aperture of diameter D and focal length z_0 the minimum beam waist can be calculated as

$$w_0 = \frac{4}{\pi} \frac{z_0 \lambda}{D\,(\cos\theta)^2} \quad (3)$$

Where θ is the angle between the optical axis of the aperture and the vector defined from the aperture centre to the position of the focus.

As said before, due to diffraction phenomenon, the beam waist will not remain constant as it varies along the propagation direction. It can be mathematically described as

$$w(z) = w_0 \sqrt{1 + \left(\frac{z}{z_R}\right)^2} \tag{4}$$

With the Rayleigh length,

$$Z_R = \frac{\pi w_0^2}{\lambda} \tag{5}$$

Which determines the length over which the beam can propagate without diverging significantly.

By analysing the equation (5), at the position z=0, the beam waist will have its minimum value, the focus of the beam, and the phase profile is flat [29].

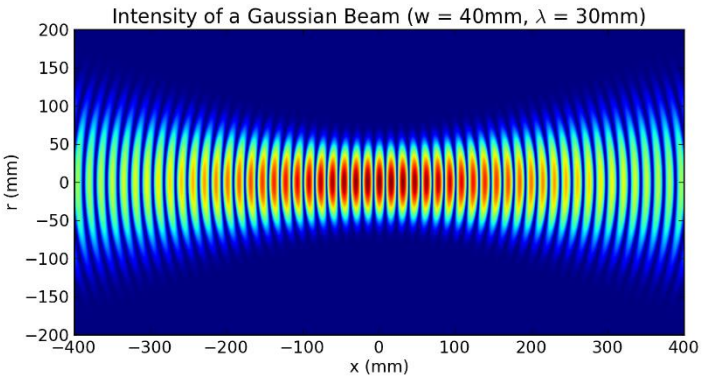

Figure 10 – Gaussian beam intensity evolution through position x. Where the intensity is maximum is where the beam waist hits its minimum [44]

3.2. Phase Shift

Through a feed, located at a focal point, a spherical wave is transmitted and will focus on a surface S, where the lens of the reflect array is located, and that will receive the fields of that incident wave.

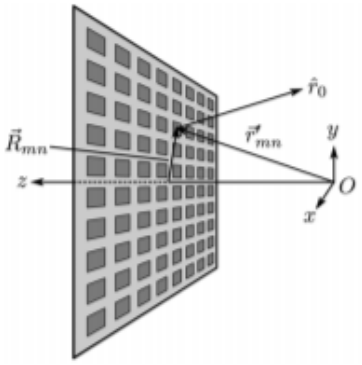

Figure 11 - Reflect array geometry with feed position [41]

Since it is a spherical wave, as mentioned before, once it focuses the RA, due to its curvature, it will not focus on every point with the same phase, besides the fact that the rays originated from the feed do not have all the same direction when illuminating the RA. The result is a RA with

points with different phases, when the goal is to reflect a wave with the same phase in all its points.

The total phase is originated according two important factors: the phase of the incident electric field on the RA and the phase shift added by the RA itself when the wave is reflected.

In Cartesian coordinates, the following equation,

$$r = \sqrt{(x - x_{feed})^2 + (y - y_{feed})^2 + (z - z_{feed})^2} \tag{6}$$

Can be defined as the distance between the feed and a point on the RA surface [(x,y,z) being the coordinated positions of every point throughout the surface].

Since the main goal is to reflect a wave with a plane phase to a specific point,

$$r_1 = \sqrt{\left(x - x_{focus1}\right)^2 + \left(y - y_{focus1}\right)^2 + \left(z - z_{focus1}\right)^2} \tag{7}$$

$$r_2 = \sqrt{\left(x - x_{focus2}\right)^2 + \left(y - y_{focus2}\right)^2 + \left(z - z_{focus2}\right)^2} \tag{8}$$

The previous equations describe, respectively, the distance from the centre of the feed aperture to the RA and from the RA to the focal specific point where the wave, or the Gaussian beam, will focus.

Defining the position of the feed, with the RA centred at the origin of the Cartesian axis,
Where Z_{focus1} can be renamed F_{IN} and Z_{focus2} as F_{OUT}, as well as X_{focus1} as *a*, since the feed will have an offset to the origin, the original equations became:

$$r_1 = \sqrt{(x - a)^2 + y^2 + (z - F_{IN})^2} \tag{9}$$

$$r_2 = \sqrt{x^2 + y^2 + (z - F_{OUT})^2} \tag{10}$$

Notice that both feeds are aligned in the y-axis, as well as the x coordinate of the second feed, which means that this second feed is aligned with the origin of the RA.

The distance from the feed to the second focal point can be defined as:

$$r_{total} = r_1 + r_2 \tag{11}$$

It is now possible to define the electric field phase distributions, φ, when the wave focuses on the RA and when it is reflected [7].

$$\phi_1 = -k_0\sqrt{(x - a)^2 + y^2 + (z - F_{IN})^2} \tag{12}$$

$$\phi_2 = -k_0\sqrt{x^2 + y^2 + (z - F_{OUT})^2} \tag{13}$$

Having defined the electric field phase distributions, which must be negative as they represent the distancing of the wave from the feed, it is now vital to add the phase shift added by the RA itself [7]. The phase correction expression results from applying the condition

$$\phi_1 + \phi_2 + \phi_{lens} = constant \tag{14}$$

Which leads to

$$\phi_{lens} = -\phi_1 - \phi_2 + constant \tag{15}$$

Therefore, the phase correction expression applied on the 30 cm x 30 cm RA can be defined as

$$\phi_{30lens} = k_0 \left(\sqrt{(x-a)^2 + y^2 + (z - F_{IN30})^2} + \sqrt{x^2 + y^2 + (z - F_{OUT})^2} + xsin\,\alpha_0 \right) \tag{16}$$

In the case of the 10 cm x 10 cm RA, the expression does not need to take into consideration the focusing distance of the beam. The beam can be considered a collimated one, reducing its expression to

$$\phi_{10lens} = k_0 \left(-\sqrt{(x-b)^2 + y^2 + (z - F_{IN10})^2} + xsin\,\alpha_0 \right) \tag{17}$$

Furthermore, when checking the phase on each point of the RA, since the phase range goes from zero to 360 degrees, there can be some adjacent points where there are phase jumps of 360. These jumps are called zoning cases and must be prevented.

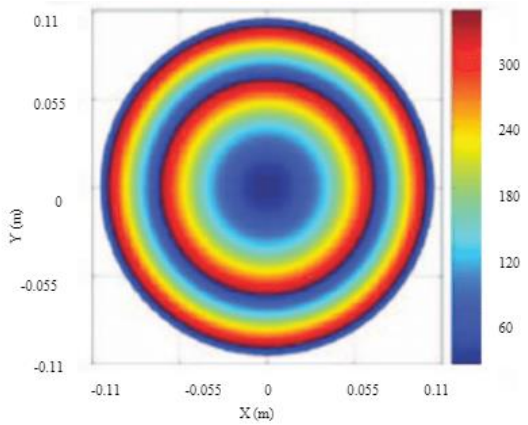

Figure 12 - Example of a required phase shift at a reflect array surface [42]

Defining ρ as the distance between a point on the aperture and the projection of the feed on the plan xy (z = 0),

$$\rho = \sqrt{(x - x_{feed})^2 + (y - y_{feed})^2} \tag{18}$$

It is possible to ensure that for a ρ smaller than a defined jump ray, the RA surface will be in zoning, otherwise that situation will not be considered.

3.3. Near Field

It is usual to define the area surrounding an antenna with three distinct regions: the reactive near field, the radiating near field (Fresnel) and the far field. Although it can be possible to define the boundaries between each region, they do not evidence abrupt changes nor are unique; they vary according to the antenna.

For the two near-field regions, the reactive one is the portion of the near-field region immediately surrounding the antenna since it is there where the reactive field predominates. It can be delimited by the boundary condition,

$$R < 0.62\sqrt{D^3/\lambda} \tag{19}$$

Which defines the distance from the antenna surface, being λ the wavelength and D the largest dimension of the antenna.

The radiating near field is delimited between the reactive near field and the far field. In this area, radiation fields are predominant, and the angular field distribution depends on the distance from the antenna. However, this area may not exit if the maximum dimension of the antenna is not larger than the wavelength. When focusing the antenna at infinity, it is usual to refer this area as the Fresnel region.

The boundaries that separate this radiating near-field from the far-field is defined by the condition

$$R < 2D^2/\lambda \tag{20}$$

Therefore, it is possible to delimit this region.

$$0.62\sqrt{D^3/\lambda} \leq R < 2D^2/\lambda \tag{21}$$

Another way to define the boundaries between near field and far field is through free space impedance. Whatever the frequency of the antenna is, at a distance λ away from the source, the impedance of all waves approaches the impedance of free space, 377 Ω, giving the distance as the wavelength. Therefore, at the distance λ/2π from the feed, we will have the transition region between near field and far field [30].

In the whole near-field region, all the waves and their nature are dependent on the distance to the antenna.

While in the reactive area, the E and H fields are the strongest and can be measured separately, in the radiating area the fields begin to radiate which weakens the fields strength [31].

The third and final region is called the far field, where the angular field distribution is independent of the distance from the antenna. According to the outer boundary of the radiating near-field region, the far field occurs from distances to the antenna higher than $2D^2/\lambda$, being the outer boundary at infinity [30].

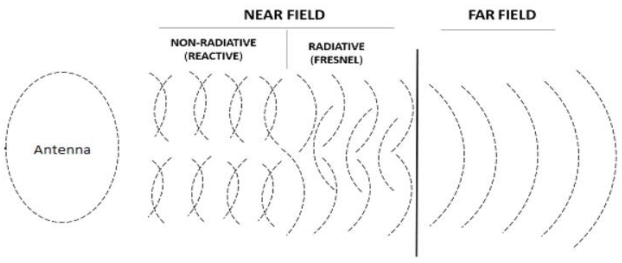

Figure 13 - Different zones of the field according to its distance to the antenna [43]

3.4. Maximum Directivity

The maximum directivity of the principal lobe of the radiation pattern is another important parameter to consider. The directivity of the lobe, the ratio of the radiation intensity in a given direction from the antenna to the radiation intensity averaged over all directions, is the value that will stand when checking if the lenses are working properly, thus, as well as the direction of the radiation pattern, the one to take more focus on.

In other words, directivity can be defined as the comparison between the radiation intensity of the antenna and a hypothetic isotropic antenna that radiates at the same power to all directions [30].

$$D(\theta,\varphi) = \frac{U(\theta,\varphi)}{< U >} \tag{22}$$

Being <U>,

$$< U >= \frac{P_{rad}}{4\pi} \tag{23}$$

Which leads to

$$D(\theta,\varphi) = \frac{4\pi\, U(\theta,\varphi)}{P_{rad}} \tag{24}$$

For a non-specified direction, it implies the maximum radiation direction,

$$D_0 = \frac{U_{max}}{< U >} = \frac{4\pi\, U_{max}}{P_{rad}} \tag{25}$$

For a given RA with dimensions *a* and *b*, it is possible to define both U_{max} and P_{rad} as

$$U_{max} = \left(\frac{ab}{\lambda}\right)^2 \frac{|E_0|^2}{2\eta} \tag{26}$$

$$P_{rad} = ab\,\frac{|E_0|^2}{2\eta} \tag{27}$$

After considering the angle $alfa_0$ that the reflected beam does with the RA, it is possible to, finally, resume the expression to

$$D_{max} = 4\pi \frac{(ab){f_0}^2}{c^2}\, sin\,(alfa_0) \tag{28}$$

4. Formulation and methods

4.1. Overall geometry problem

For the wireless power transfer between the two satellites, the implemented geometry needs to take into account the size of the RAs, the position of the feeds (and their distance to the RAs), the distance between both satellites, as well as the beam waist.

Due to the cubesats small dimensions, the feeds must be close to the RAs. At the same time, they must be positioned outside the beam range to avoid interferences within the reflection phenomenon. Therefore, to guarantee that this study could be successfully completed, the following geometry is used:

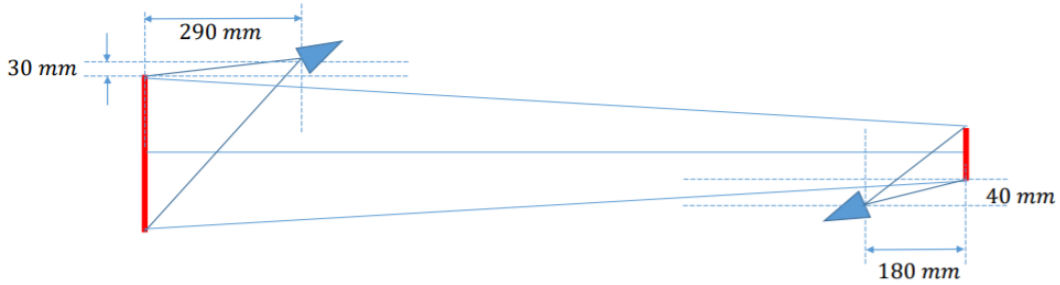

Figure 14 - Full geometry of the problem

For the RAs, the biggest one has a total area of 30 cm x 30 cm, with the 3U cubesat having a volume of 10 cm x 10 cm x 30 cm (30 cm height). This means the RA area surpasses the total area of the largest face of the cubesat, which is of 10 cm x 30 cm. Since the cubesat needs to be as much compacted as possible [32], for it cannot surpass the total volume of the satellites, the solution is to divide the RA into 3 sections that will be folded for the launch of the cubesat. Once it reaches space, the sections will be deployed into their final positions.

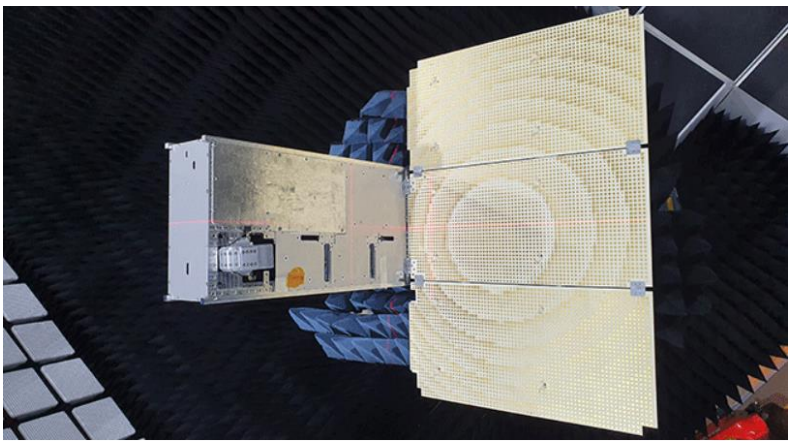

Figure 15 – Example of a deployable reflect array antenna for a cubesat [32]

From the bigger satellite, on the left side of Figure 14, the feed will radiate the beam to the RA surface to then be transmitted. Once it is transmitted, it will travel a certain distance, approximately 1.5 meters, until it gets to the second RA, attached to the smallest satellite. After this, the process is similar, though in the reverse direction, since this time the RA will reflect the light beam back to the second feed, positioned near it.

The first feed is positioned 180 mm of the centre of the RA and at a height of 290 mm, while the second feed will be 90 mm distanced from the RA centre and at a height of 180 mm.

4.2. Reflect Arrays dimensions

The sizes of the RA are according to the sizes of the satellites. While they are both CubeSats, nanosatellites, this process involves two different sizes: the biggest one with a dimension of 3U, to accumulate more energy to be transferred, and a smaller one with a dimension of 1U. This is the basis of this work since the main goal is to check the viability of wireless power transfer between two satellites.

The first satellite, the biggest one, required a larger RA surface due to its size. This satellite, with dimension 3U, has the triple of the height of the second one, with its RAs area being also the triple the size of the smaller RA. For a 1U dimension CubeSat, the area of the RA surface is 10 x 10 cm, so the area of the biggest RA is 30 x 30 cm. Both RAs will then be attached to CubeSat faces to be deployed after launch, as mentioned and explained on the previous sub chapter.

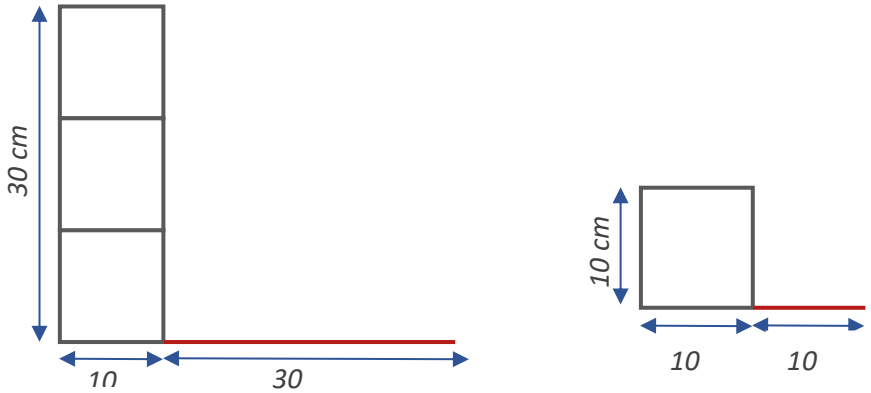

Figure 16 - Dimensions of the 3U CubeSat, with the RA in red (right); Dimensions of the 1U CubeSat, with the RA in red. xz plane view

4.3. Feeds dimensions

The feeds are responsible for the transmission and reception of the beam, while the RAs just complete the process by reflecting it to the desired directions.

Until now, the feeds have been considered as focal points near the RAs. However, they are in fact horn antennas, composed by a wave-guide that will generate the beam, and an aperture to radiate it. Their size will affect the maximum directivity of the beam. For a horn antenna positioned symmetrically to the z-axis, it will have its maximum propagation on the z direction.

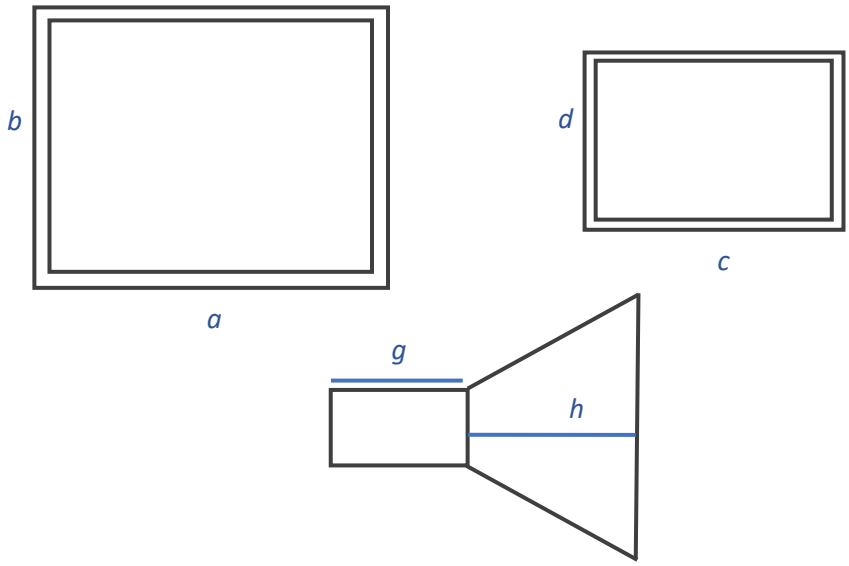

Figure 17 - sizes of the horn antenna: horn antenna aperture (top left); waveguide size (top right); horn antenna length (bottom)

The full length of the horn is composed by the horn itself, with a length (dimension h) of 46.0465 mm and the length of the waveguide, g, of 20.974 mm (dimension g), making a total length of 67.0205 mm.

For the waveguide, the base dimensions are 12.668 (dimension d) and 6.318 (dimension c), while the horn antenna aperture has an area of 30.5 (dimension a) over 23.16 (dimension b) millimetres, as shown in Figure 17 (top left and right). Both aperture and waveguide base have a 1 mm thickness.

4.4. Reflected and Incident angles

The first feed, corresponding to the one near the biggest RA (Figure 16) will radiate the beam light focusing the RA with a specific angle. This angle, α (Figure 18.), is dependent on the position of the feed regarding the position of the RA. Using the Pythagoras Theorem, it is possible to determine the angle:

$$\alpha = \tan^{-1}\left(\frac{18}{29}\right) = 31.83° \quad (28)$$

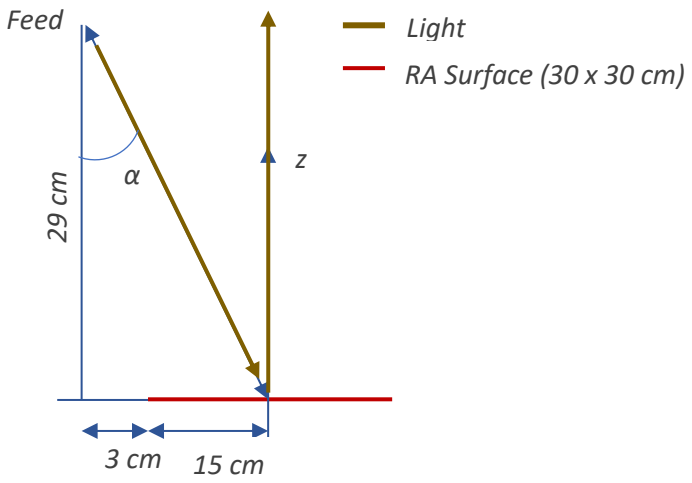

Figure 18 - Beam hitting the biggest RA and being reflected to travel the distance between RAs.

From Figure 18, the beam reflected by the biggest RA will be radiated linearly with its geometry, meaning, the reflected angle will be zero and the light beam direction will be perpendicular to the RA surface. For this reason, feeds must not be on the line of sight of the beam direction, from one satellite to another. Therefore, the feeds position where decided and presented as in Figure 16.

Now for the second feed and the beam reflected by the smallest RA, the reflected angle also depends on the position of the feed. The following figure will represent the geometry of this problem:

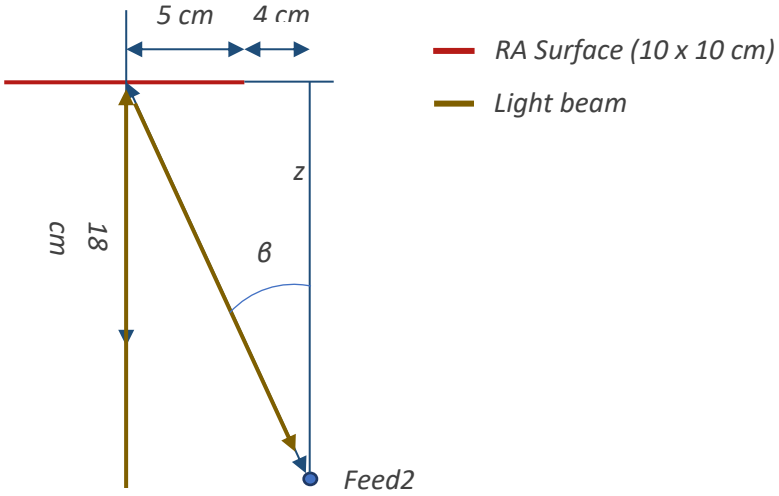

Figure 19 - light beam that hits the smallest RA and it is then reflected towards the second feed

In this case, the reflected angle, by simple calculations, is:

$$\beta = \tan^{-1}\left(\frac{9}{18}\right) = 26.57° \tag{29}$$

The distance between the two satellites, meaning, the distance the beam reflected by the biggest RA will travel until it gets to the smallest RA, is 1.5 m. This distance defines the region where the satellites will work as the near field, where the waves and their nature are dependent on the distance to the antenna. This will make the difference between being possible to focus a Gaussian beam or having collimated rays (the rays leaving the edges of the RA's surface are parallel).

5. Design and simulation results

To obtain the Gaussian beam, it is necessary to define the phase shifts of the RAs and, more specifically, of the unit cells. This also affects the direction of the reflected beam, so it is mandatory to define the phase laws related to each antenna.

Since both RAs are filled with unit cells, responsible for the phase correction, it is important to define the desired phase for each cell, to reflect the beam with both desired direction and phase.

To present a full structured study over all the aspects of the geometry, as well as to better understand the inputs and outputs of the whole system, from one satellite to another, the process was divided in two problems: the beam being transmitted by the first feed and being reflected by the first RA, towards a specific focusing point, where the second RA is positioned, Figure 20:

Figure 20 - Geometry of the first problem

Together with the second problem where the already reflected beam hits the second RA, being then reflected towards the second feed, Figure 21.

Figure 21 - Geometry of the second problem

5.1. Phase laws

To achieve the desired Gaussian beam, each unit cell, located at a different position of the RA, must compensate the phase difference from the centre of the RA.

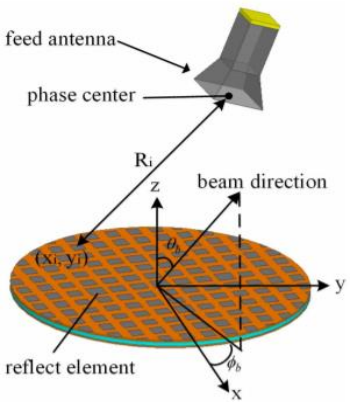

Figure 22 - reflect array antenna diagram.

Once the beam is radiated from the feed to the larger RA, since it is a spherical wave, has seen before, the beam will not focus on every point of the RA surface with the same phase. Therefore, it is mandatory, to achieve a reflected wave with a plane phase when it leaves the lens, to make a phase correction, called phase shift.

From the sub chapter concerning the phase shift, presented earlier, and with the positions and sizes of the RAs and feeds, it is possible to change and implement the new phase equations.
The field phase distributions, φ, when the wave focuses on the 30 cm x 30 cm RA and when it is reflected are

$$\phi_1 = -k_0\sqrt{(x-18)^2 + y^2 + (z-29)^2} \tag{30}$$

$$\phi_2 = -k_0\sqrt{x^2 + y^2 + (z-150)^2} \tag{31}$$

In addition, the phase shifted added by the RA is

$$\phi_{lens} = k_0\left(\sqrt{(x-18)^2 + y^2 + (z-29)^2} + \sqrt{x^2 + y^2 + (z-150)^2} + xsin\ 0\right) \tag{32}$$

Which leads to

$$\phi_{lens} = k_0\left(\sqrt{x^2 + y^2 + (z-29)^2} + \sqrt{x^2 + y^2 + (z-150)^2}\right) \tag{33}$$

Being the total phase the sum of the three previous equations.

$$Phase_1 = \phi_1 + \phi_2 + \phi_{lens} \tag{34}$$

Then, after the phase shift, the beam will travel 1.5 m until it hits the second RA. Here it will have, again, a phase shift. While on the first occasion, the objective was to turn a spherical wave into a Gaussian beam (plane phase), on this situation it is the opposite. The phase shift that the second RA will add must fulfil the outcome of radiating to the second feed a spherical wave.

To achieve the phase shift expression for the second RA, corresponding to when the reflected wave hits the second RA and it is then reflected to the second feed, it is used the similar process.

$$\phi'_2 = k_0\sqrt{(x-9)^2 + y^2 + (z-18)^2} \tag{35}$$

And the phase shift imposed by the second RA

$$\phi'_{lens} = k_0\left(\sqrt{(x-9)^2 + y^2 + (z-18)^2}\right) \tag{36}$$

5.2. Simulation Tools

Before making any type of simulations of the whole system as a prototype, it was important to make calculations and use certain tools that allowed to simulate the system and determine different aspects of it. For this, different simulation, computation, and 3D tools were used to follow a certain number of steps before the final execution.

Initially, KH3D_near [33] code was used to determine, for an arbitrary feed position, RA size and shape (either in rectangular or spherical coordinates), as well as an arbitrary distance from the aperture, the magnitude and also the phase of the incident beam wave on both RAs. This helped understanding better how the positions of the feed and the sizes of the RAs, as well as distances, affected the directivity of the antennas. It also showed the behaviour of the beam throughout the distance between the satellites, to determine if the directivity and beam waist were according to the desired values.

After the first steps with KH3D [33], CST Microwave Studio (CST_MWS) [34] was used to simulate a 3D model of all the possible types of unit cells, computing the phase distribution and magnitude for different sizes, to analyse the reflection factor of each cell.

After the unit cells were optimized, with Mathematica, a code was used to calculate the required phase distribution along the whole RAs for each unit cell, to create a reflector capable of defining a specific direction for the beam. Using a Visual Basic Script (VBA) created to implement a macro to be used in CST_MWS, RAs were designed and populated with the already studied unit cells, to be simulated with the respective feeds, to evaluate their performances in terms of directivity, gain, beam steering as well as radiation patterns. With this program, it was also possible to simulate different types of antennas, from horns, reflect arrays, wire antennas, etc. In this case, horn antennas were designed and simulated as feeds to check their directivity, comparing it with the directivity calculated with KH3D.

With both antennas designed, it was time to simulate, in time domain, the combination of the RAs with the respective horn antenna.

5.3. Transmit array examples

The whole process' behaviour is simulated with the use of a Mathematica notebook. Transmit arrays are used, since they work with the same phase shift method way as reflect arrays. For the simulations matter, both TAs and feeds are defined for specific positions and sizes to implement the idea of the phase shift. The objective is to simulate a planar RA to produce a Gaussian beam.

The definition of the initial conditions is a crucial step. The horn antenna has a gain of 16 dB, with the two RAs widths being of 30 cm for the largest RA, and 10 cm for the small one. For the antennas distance in consideration, 1.5 m, the best approach is to have higher frequencies. However, when focusing on the smallest RA, the spill over must be avoided. Therefore, the antennas must have high gains for that purpose. On the other hand, antennas with high gains means they will be large in terms of wavelength, another reason why the frequency must be as high as possible.

Another factor to take into consideration is the conversion efficiency from radio frequency to DC (direct current), since it drops with the increase of the frequency.

Considering all these factors, a reasonable frequency value would be between 20-30 GHz. For this reason, the 24 GHz frequency was chosen to proceed with the study.

Since the 30 cm x 30 cm RA is the origin from which the beam leaves towards the focusing spot, it is now possible to calculate the minimum beam waist according to the equation (3),

$$w_0 = \frac{4}{\pi}\frac{z_0\lambda}{D\,(\cos\theta)^2} = \frac{4}{\pi}\frac{150 * 1.25}{30\,(\cos 0)^2} = 7.96\ cm \tag{37}$$

Which presents a good diameter for focusing on the 10 cm x 10 cm RA, avoiding this way the spillover phenomenon.

Considering the focus distances of the feeds to the apertures, the result is a beam focused near the centre of the RA, since the angle of the feed makes the beam focus with different phase along

the RA, both in magnitude and phase. This was a crucial step to define the phase laws for each unit cell implemented on the RA, from their phase difference from the centre.

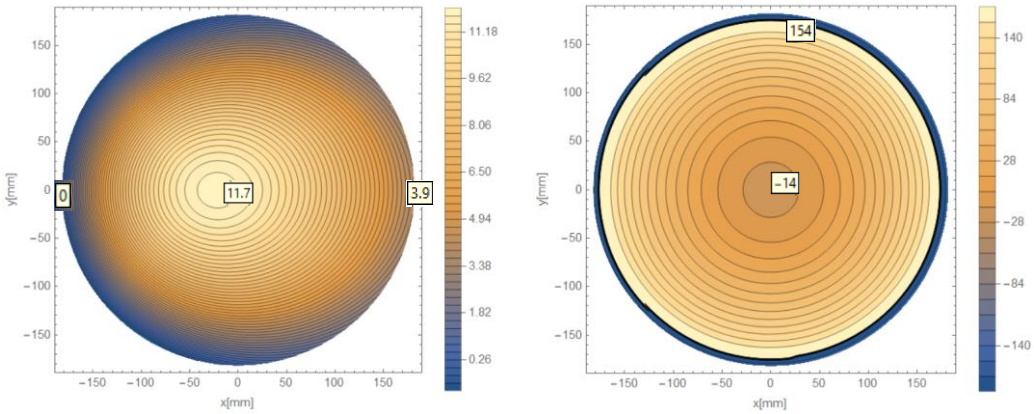

Figure 23 - beam focus on the 30x30 cm RA: left side directivity in dB on the RA; right side phase distribution of the beam on the RA

For the magnitude, the tapper between the centre and the edge of the lens is approximately 10 dB, the value established in the begging of this work as the target value to achieve. It is also possible to infer, from the right side of Figure 23, that the wave does not hit the lens with the same phase in every point, proving the need to add a phase shift on the surface to allow reflecting a planar front wave.

After the phase correction provided by the lens, the beam wave focuses at 1.5 m, meaning it has its lowest beam waist at this point and, consequently, maximum directivity. The phase is planar, confirming the phase shift of the initial spherical wave.

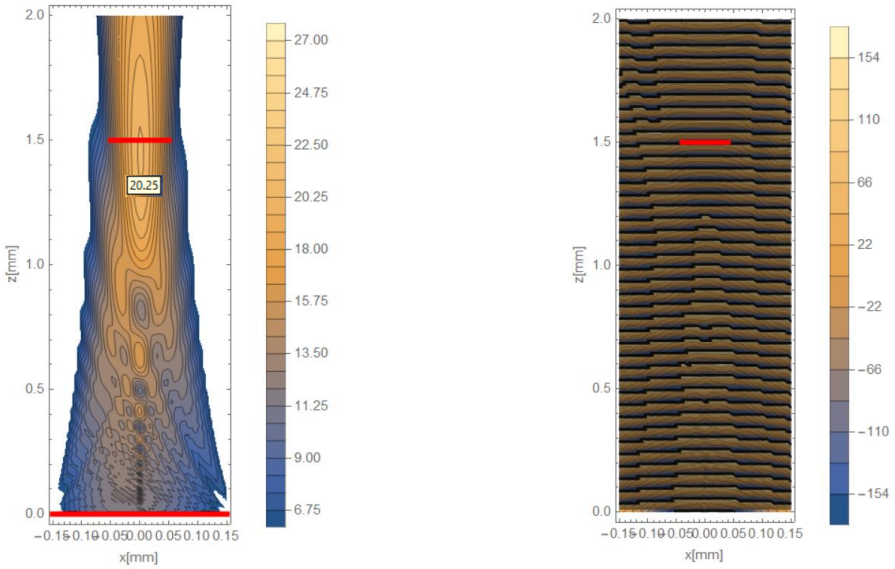

Figure 24 - Beam wave reflected by the biggest RA and focusing on the second RA: Gaussian Beam directivity across the 1.5m distance (left side); Gaussian Beam planar front wave phase across the 1.5m distance (right side).

For this lens, for later check results purposes, the maximum directivity, according to the sizes of the lens itself and the expression given in (27), calculated on the same mathematica notebook, is 38.1 dB.

The second lens, as shown in Figure 25, gets the beam focused right on the centre of the lens, since there is no angle on the beam from the biggest lens to the smallest one, avoiding the

maximum spill over possible from the edges. Since the beam wave is a planar one, the phase is almost constant throughout the lens, before the new phase shift imposed by the second lens.

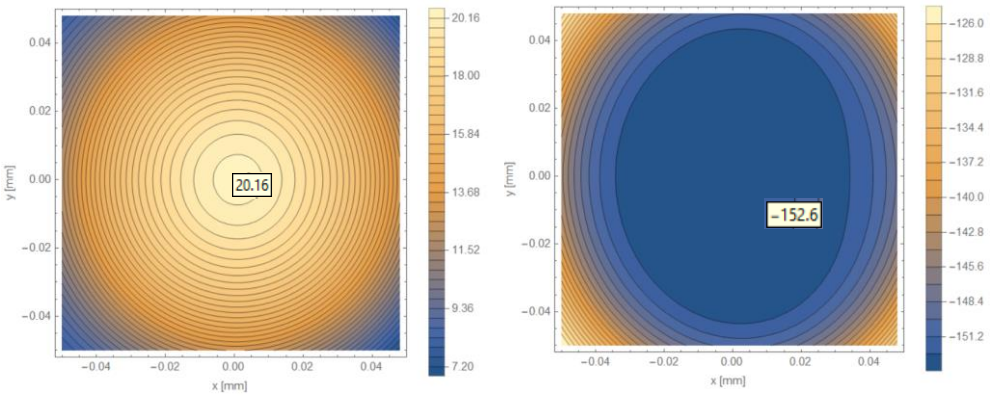

Figure 25 - Beam wave reflected by the biggest RA and focusing on the second RA: Gaussian Beam directivity across the 1.5m distance (left side); Gaussian Beam planar front wave phase across the 1.5m distance (right side).

The beam that leaves the second lens is already a spherical wave, which means that, after the phase correction, the beam phase presents an angled beam direction, to hit the second feed position, and a phase distribution that, different from before, is as it is shown in Figure 26 and Figure 27. Both figures represent the total phase of the wave that leaves the second RA towards the second feed.

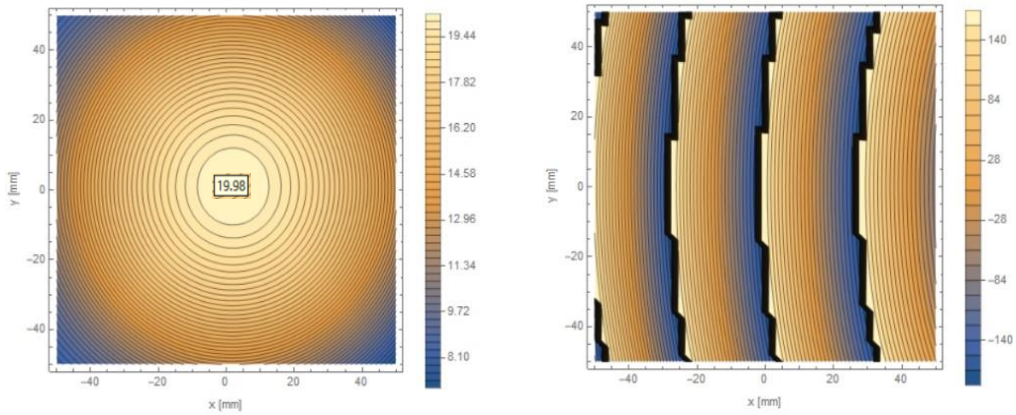

Figure 26 - Second RA magnitude and phase after the phase shift. [XY plane]

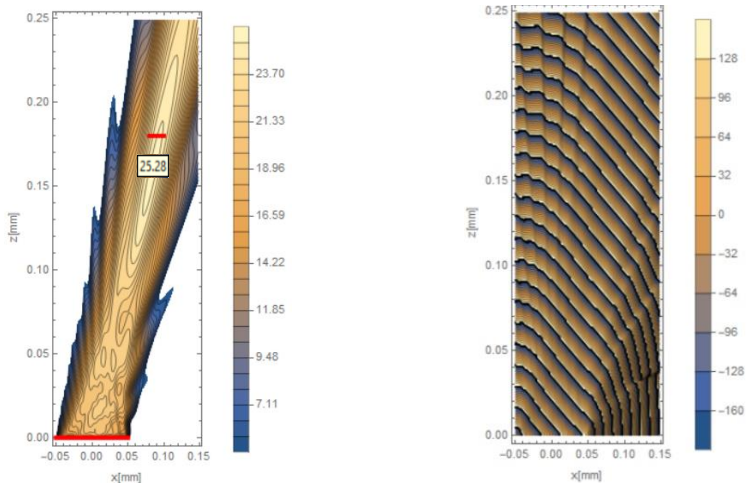

Figure 27 - Gaussian Beam that exists the RA and focuses on the feed (left side - magnitude, right side - phase) [XZ plane]

Again, for this lens, and using expression (27), the maximum directivity is calculated.

5.4. Unit Cells design and simulation

Both lenses are filled with unit cells, components that not only allow to have a better reflection, as well as providing the phase shift needed to transform a spherical wave into a plane wave (and vice-versa) and to steer the beam to the desired direction.

The design is composed of a PEC base (a metal material), a substrate material and finally two copper rings, one outer and one inner, that will be modified for the phase range needed.

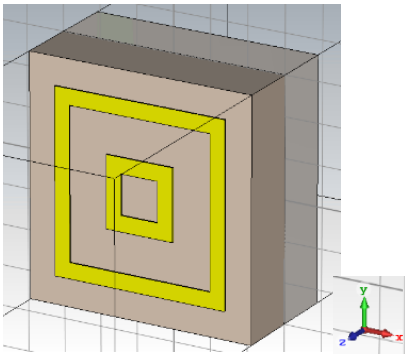

Figure 28 - Perspective of the 3 different types of materials that compose the unit cells

Since each unit cell as dimensions of 3 cm over 3 cm, both substrate and metal, it needed to check those same dimensions. In addition, both have the same thickness (z-axis), of 0.787 cm, with the substrate, called Rogers RT5880 (lossy), having a 2.2 permittivity.

The square rings are made of copper (pure). This means that they have an electric conductivity of 5.96e +07 [S/m].

For the simulations, the three parameters of the unit cell's rings vary to successfully achieve a 0 to 360 degrees range, a full coverage of the entire phase spectrum to be able to shift the phase. As shown in Figure 29, r_{01} represents the dimension of the outer ring's size, r_g is the gap between both rings and r_w is the thickness of both rings.

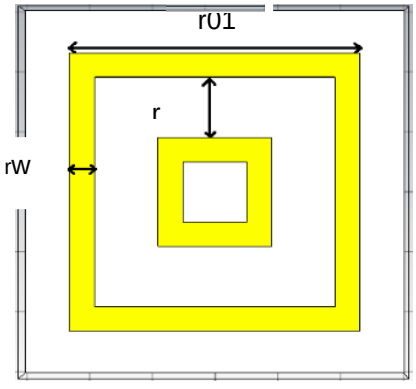

Figure 29 - different dimensions of the unit cell to be tested

The simulations were executed on CST_MWS. The scattering parameter usually describes the power transfer between two ports. For instance, since we are dealing with an antenna, a common one-port network, it will be a 1x1 matrix, meaning that S_{11} will indicate the amount of radiated or dissipated power by the antenna. More specifically, it is necessary to verify both magnitude and

phase of the S_{11}: magnitude (dB) since it is important to have results has near to zero as possible (and no higher than -0.5 dB), and phase because the objective, as mentioned before, is to have a full 0 to 360 degrees range, with phase jumps no higher than 60 degrees.

The r_g and the r_w parameters varied from 0.1 to 0.5 cm, while r_{01} varied from 0.2 up to 2.9 cm, to obtain all the possible unit cells designs for the phase range.

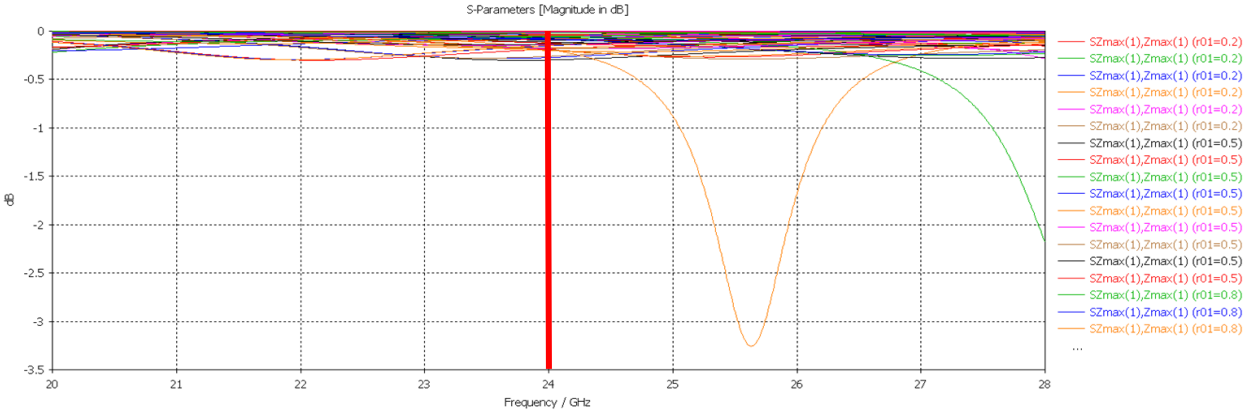

Figure 30 - S11 magnitude simulated for the unit cells parameters variation at 24 GHz

From Figure 30, at 24 GHz the magnitude of the S_{11} parameter clearly varies from zero to -0.5 dB, which means that the majority of the light is reflected on the unit cell, having low energy losses.

Without this magnitude results, it would be irrelevant to have a full phase range coverage, since the unit cells tested would not be accurate enough.

Now, for the phase testing, at 24 GHz, as mentioned before, it is mandatory to have no more than 60 degrees jumps.

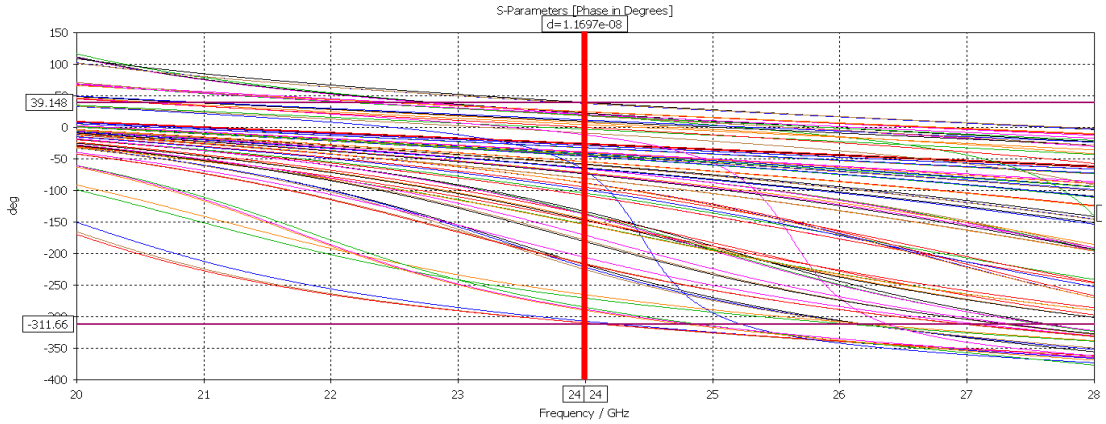

Figure 31 - S11 phase simulated for the unit cells parameters variation at 24 GHz

As shown in Figure 31, at 24 GHz, the different phase jumps, because of the variation of the S_{11} parameter, cover a degree spectrum from 39.148 to -311.66 degrees, completing the 360 degrees range necessary to completely cover the arriving wave that hits the lens with different phases across the surface. Since the maximum degree jumps accepted to have a validated simulation were stipulated at no higher than 60 degrees, even though there are areas where the phase jumps leave bigger gaps than in other areas, overall, it can be concluded that the degrees' simulation results were satisfactory to validate the unit cells.

Having the unit cells dimensions established, as well as the phase range, the following step is to calculate the jumps, define the phase range for 0 to 360 and put it all on a table to be easier to analyse the obtained data.

R01	RW	RG	Magnitude	Phase	Phase jump	Conversion to 0-360 (+320)
2.6	0.3	0.5	-0.04	-310	-	10
2.4	0.1	0.1	-0.19	-285	25	35
2.6	0.5	0.1	-0.08	-266	19	54
2.3	0.1	0.5	-0.26	-226	40	94
2.4	0.3	0.1	-0.18	-207	19	113
2.3	0.2	0.5	-0.18	-182	25	138
2.4	0.5	0.5	-0.09	-154	28	166
2.2	0.1	0.1	-0.19	-135	19	185
2.3	0.5	0.5	-0.05	-109	26	211
2	0.1	0.1	-0.04	-66	43	254
2	0.3	0.1	-0.02	-59	7	261
1.7	0.3	0.1	-0.006	-40	19	280
1.4	0.1	0.1	-0.003	-33	7	287
2.9	0.1	0.3	-0.02	-10	23	310
2.9	0.3	0.1	-0.008	7	17	327
2.6	0.1	0.1	-0.04	19	12	339
2.9	0.5	0.5	-0.005	25	6	345
2.8	0.5	0.1	-0.04	39	14	359

Table 3 - Unit Cells dimensions, magnitude, and phase definitions

5.5. Horn/Feed simulation

Alongside with the need to implement the unit cells on the lens, it was also needed to create the horn that will radiate the beam to be reflected. The definition of the horn is different for both lenses, since, due to its positions, the angle of which the beam will be radiated is different. It is already known, from Figure 18 and Figure 19, and from equations (28) and (29), the defined radiated beam angles.

The next step to have in mind is regarding the datasheet for the available horns in laboratory. Since this work is done considering 24 GHz frequency, when configuring it on CST the horn must follow certain parameter values so that its simulation can be as close as possible from the laboratorial horn.

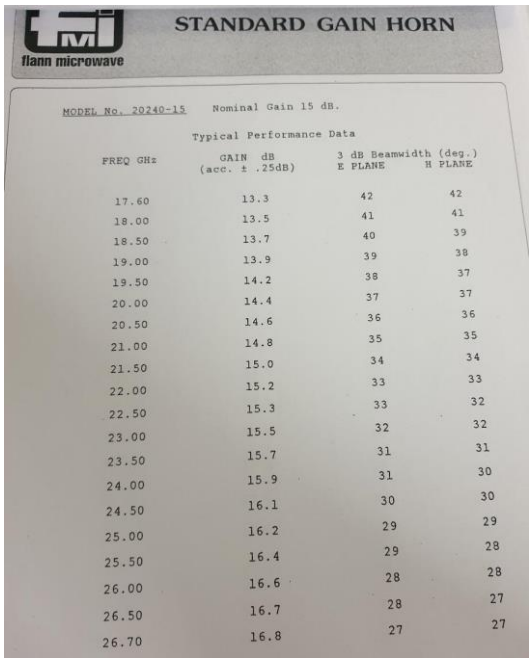

STANDARD GAIN HORN

flann microwave

MODEL No. 20240-15 Nominal Gain 15 dB.

Typical Performance Data

FREQ GHz	GAIN dB (acc. ± .25dB)	3 dB Beamwidth (deg.) E PLANE	H PLANE
17.60	13.3	42	42
18.00	13.5	41	41
18.50	13.7	40	39
19.00	13.9	39	38
19.50	14.2	38	37
20.00	14.4	37	37
20.50	14.6	36	36
21.00	14.8	35	35
21.50	15.0	34	34
22.00	15.2	33	33
22.50	15.3	33	32
23.00	15.5	32	32
23.50	15.7	31	31
24.00	15.9	31	30
24.50	16.1	30	30
25.00	16.2	29	29
25.50	16.4	29	28
26.00	16.6	28	28
26.50	16.7	28	27
26.70	16.8	27	27

Figure 32 - Datasheet of the horn to guide through the correct parameters' values.

As seen in Figure 32, the horn must have a 24 GHz frequency with a 15.9 dB gain. The Beam width at 3 dB, in degrees, must be 31 and 30, respectively for E plane and H plane. With the dimensions defined in previous chapters, the simulation of the horn is now possible to do in CST.

To execute the simulation and verify the viability of the horn, in the CST Microwave Studio, it was selected, for the project template, the Antennas option present in the MICROWAVES & RF/OPTICAL workflow (for this specific case of antennas, the waveguides, including horns, cones, etc. was selected). The time domain is selected since it provides a much faster simulation execution. Finally, the minimum and maximum frequency limits, as well as the monitors to be added, are selected.

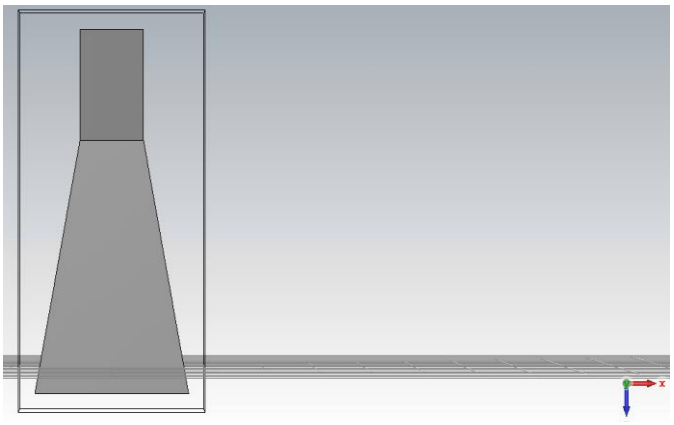

Figure 34 - Vertical horn perspective, XZ plane (I)

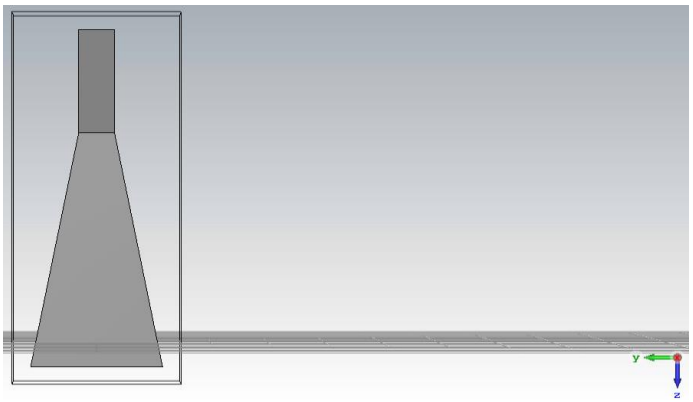

Figure 33 - Vertical horn perspective, YZ plane (II)

The ideal horn antenna, that will be used in the laboratorial phase, consists of an aperture and a waveguide combined in a vertical position and with the dimensions described earlier.

As seen in Figure 34 and Figure 33, the aperture and the waveguide are aligned with the symmetry axis, and attached together to complete the whole horn's project.

The simulation gives an overview of the way it should work, with the parameters being fulfilled according to the theoretical specifications. After simulating the horn to visualize the far field results, the horn gives a max directivity of 15.9 dB,

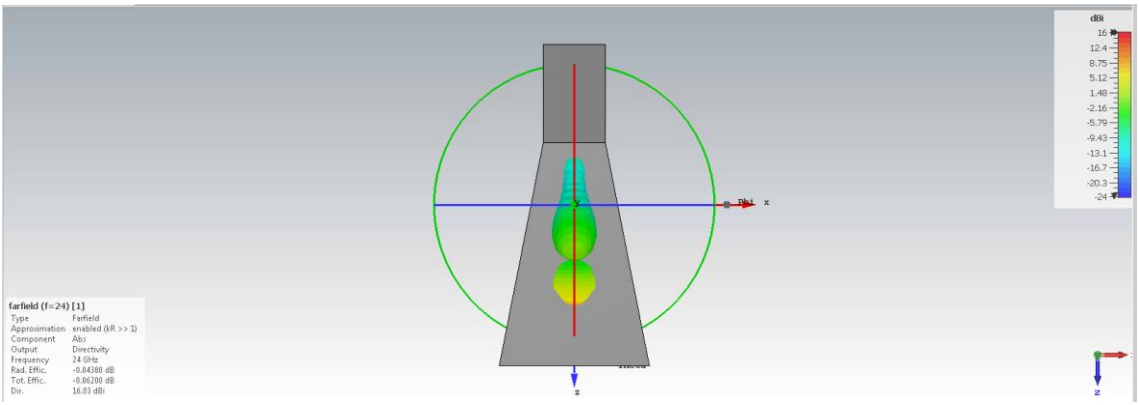

Figure 35 - XZ plane cut of the horn's 3D Far field simulation, with structure

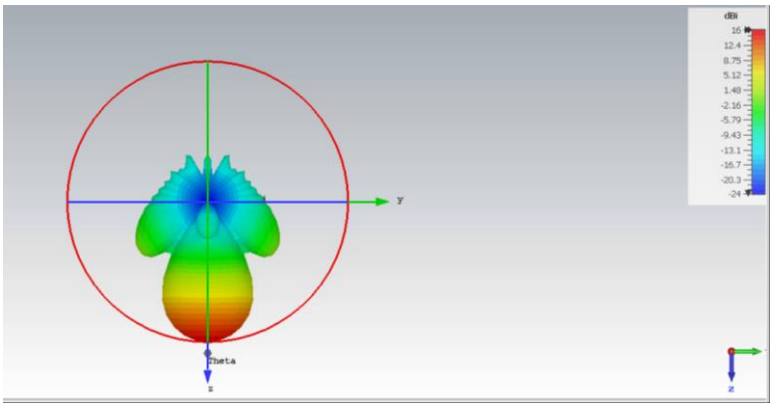

Figure 36 - YZ plane cut of the horn's 3D Far field simulation, without structure

Without the horn's structure visible, the far field's 3D result shows a clear principal lobe with the maximum directivity value, with the direction z (the direction of the aperture, meaning it has its maximum value at the centre of the horn) and two secondary lobes with almost no directivity wasted (in the perfect conditions).

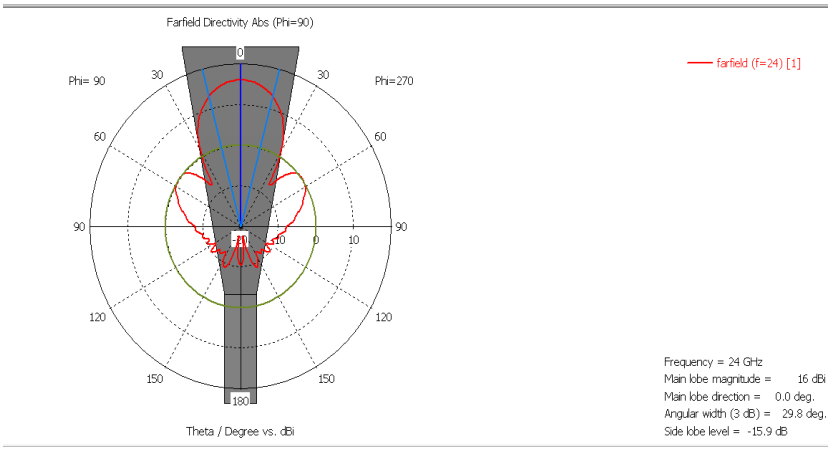

Figure 37 - Far field results in the Phi = 90 plane, with visible structure

With the Phi=90 plane cut and following the established values from Figure 37, it is possible to confirm the main lobe being at the centre of the aperture, with its values being 16 dB of Gain and Angular width at 3 dB of approximately 30 degrees.

Although this been the horn to be used in experimental results, and having the ideal results to proceed with this study, this horn cannot be used for the needed simulations. Has seen before, the feed will have an inclination angle of 31.83º towards the lens, meaning that this horn must be have that same tilt. However due to software limitations, for the CST_MWS software, the waveguide must be aligned with one of the coordinate planes, meaning it must be parallel with one of the symmetry planes.

5.6. Adapted Horn Simulation

To overcome the waveguide plane issue, it was decided to maintain the waveguide fixed and parallel to one of the symmetry planes, and to tilt the rest of the horn to have the best-approximated results. Since the aperture guides the direction of what comes from the horn, the waveguide was tilt with the necessary angle to reflect on the lens.

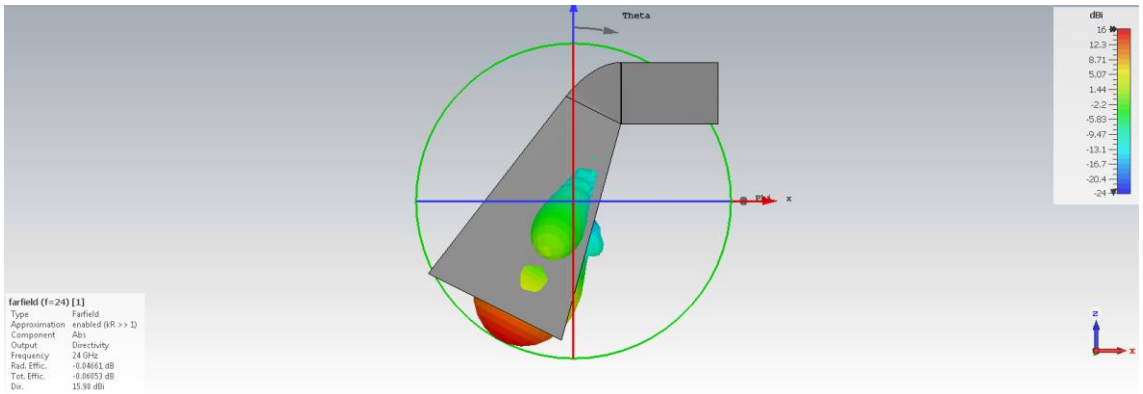

Figure 38 - Adapted Horn antenna with tilted waveguide

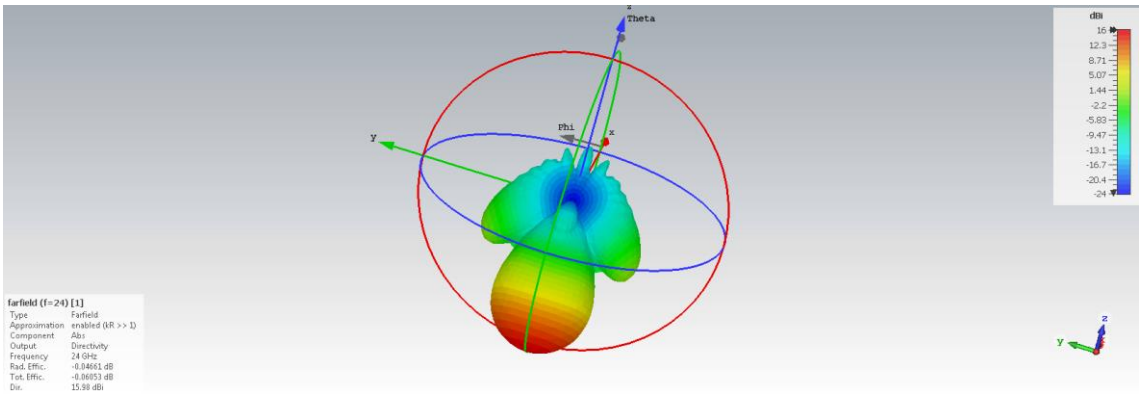

Figure 39 - Adapted horn's simulation

Has seen in Figure 38, the horn's curvature was placed at the connection between the aperture and the waveguide, to minimize the potential impact that the increase in size and deformation of the horn may have on the simulations.

The simulation proved acceptable to proceed with the study, since the horn, even having a curvature and thus slightly changing its dimensions, maintains the same maximum directivity at the same frequency.

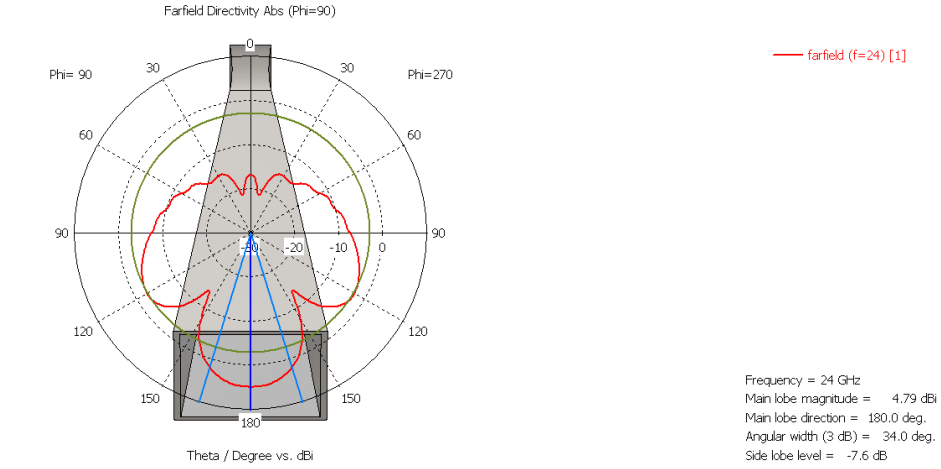

Figure 40 - Horn structure in the Phi=90 plane, and respective diagram perspective

Through another perspective, like the one in Figure 40, it is possible to understand that the main lobe direction is coincident with the aperture direction. The slight deviation of the angular width (3 dB) is due to being calculated according to the coordination axis, while the horn is tilted.

5.7. RAs configuration and parametrization

The RAs are built in the CST_MWS software through a script that is ran in the VBA Macro Editor. The script, besides defining the way the RA should be implemented, as well as the type of materials and positions, has two functions that will read two ".txt" files from the library: One with the sizes of all the possible unit cells, according to the phase shift, and one defining specifically all the positions of them. This is possible through the execution of a Mathematica notebook, where the unit cells are numbered and, defining the feed position as well as RA positions and dimensions, it generates those same ".txt" files.

In the Mathematica notebook, it is first defined the position of the feed and RA to provide the right measures and sizes of the problem. Since the RA is a square, the number of cells per line and per column are also set. With the phase shift law and the different types of cells defined, by running the notebook, it will return the graphics shown in Figure 41 and Figure 42. While Figure 41 represents the unit cells numbered from one to 18 and spread throughout the RAs area according to their phase, Figure 42 shows the phase distribution from zero to 360 range across the RAs area.

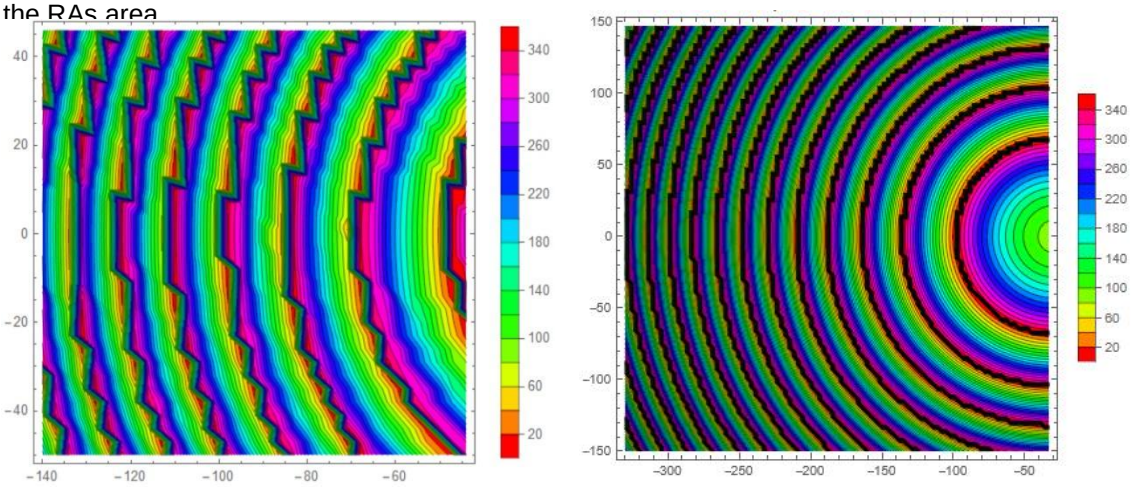

Figure 41 - RAs populated with the unit cells, numbered according to the coloured scale (18 total). 10 cm RA (left) and 30 cm RA (right)

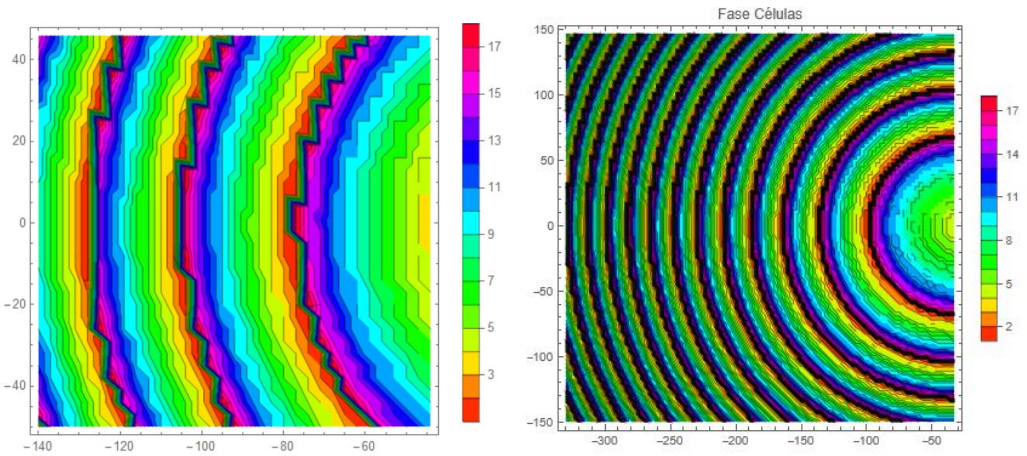

Figure 42 - Unit cells phase distribution throughout the RA surface. 10 cm RA (left) and 30 cm RA (right)

Once the two ".txt" files are generated, the next step is to create a macrocode ".bas" where all the measurements of the lens and cells are defined, as well as materials. Furthermore, two functions that will read the files and create the cells and their positions are included. The path of both files is also defined, so that when on the VBA Macro Editor, the software can fetch those same files and perform the lens construction.

5.8. RA construction and simulation

After all the calculations of the RA sizes, unit cells allocation and creation of the macro code, the study proceeds to the CST where the ".bas" file runs. The software first creates the metallic surface, on which each unit cell formed by the substrate material and the copper rings is generated. After the conclusion of the generation of the RA, it is time to allocate the horn antenna

to its geometric position and proceed with the parametric changes that allow a smoother and clearer simulation.

5.8.1. 10 cm Reflect Array

For the simulations and analysis of the RA on the CST, it is necessary to first use the KH3D to obtain a radiation pattern of the aperture to better analyse its efficiency.

According to the KH3D calculations, at 24 GHz and with the feed positioned, represented on Figure 43, the maximum directivity was achieved at 27.8 dB.

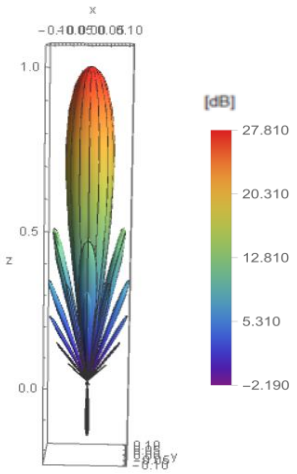

Figure 43 - 10 cm TA radiation pattern, calculated by KH3D

This radiation pattern is obtained by radiating towards an aperture surface with an edge tapper of approximately 10 dB, as seen in Figure 26 and Figure 27.

The RA is then simulated using the time domain solver of CST-MWS, resulting on the following far-field result:

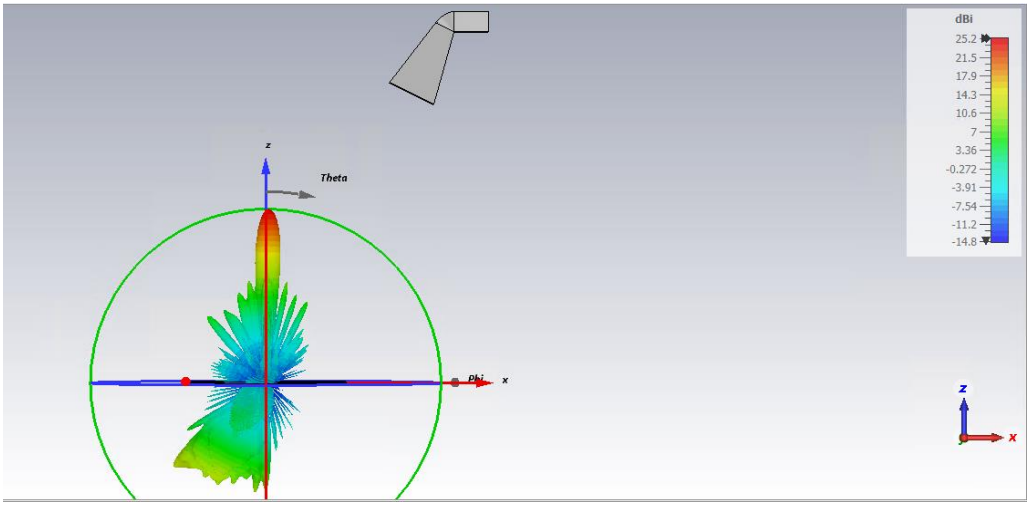

Figure 44 - far field results from a XZ plane perspective

As seen in Figure 44, the simulation results on an almost vertical main lobe, with an obtained gain of 25.2 dB (theta = 0). Comparing with the KH3D results, where the predicted directivity peak was at 27.8 dB, resulting in a difference of 2.6 dB. This far field simulation resulted on a total efficiency of -0.1855 dB, equivalent of an efficiency of 94.09%, a significant result for the antenna's performance

On a different perspective, from the YZ plane view, it is notable the symmetry of the far-field result in terms of what is reflected by the RA and what is lost in the process.

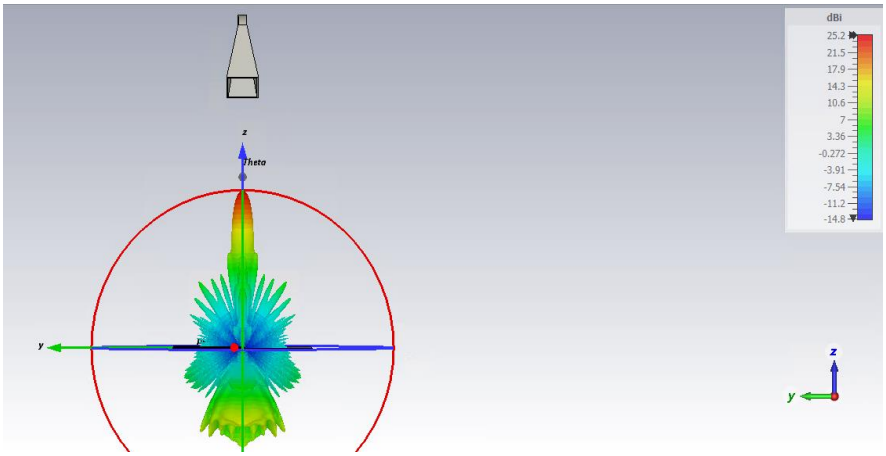

Figure 45 - far field results from an YZ plane perspective

The fact the far field on XY is not completely symmetric might be linked to human error when creating and studying the unit cells design. This led to a small angle shift on the main lobe, which also influenced the appearance of a “shoulder effect”, visible in Figure 46.

The ratio between the peak amplitude of the main lobe and the second highest side lobe, the side lobe level is of -11.5 dB.

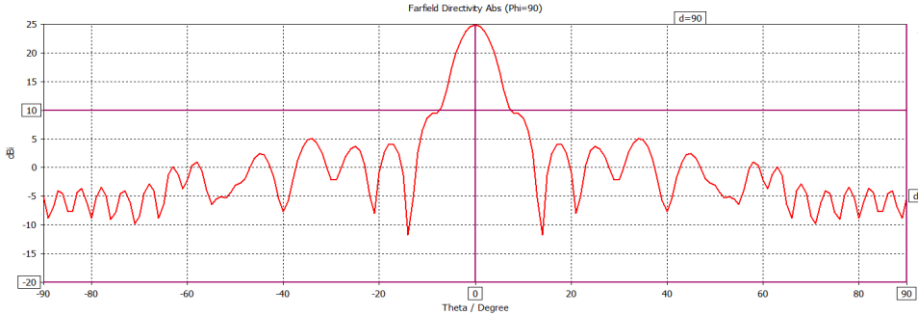

Figure 46 - Phi=90 plane for the far field simulation

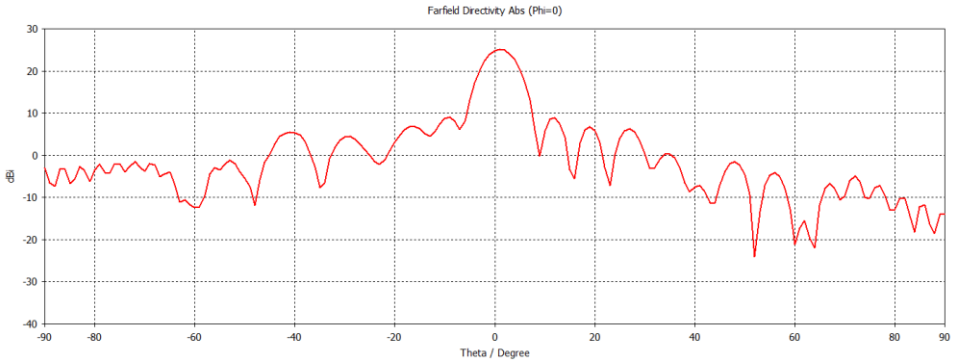

Figure 47 - Phi=0 plane for the far field simulation

While on the phi = 90 plane it is noticeable a perfectly symmetric radiation pattern, with the main lobe centred at theta = 0, on the phi = 0 plane, due to a shift of 1 degree in theta (the main lobe is centred at theta = 1), a not so symmetric radiation pattern is presented.

Although the 1-degree shift may have influenced the simulation's symmetry, it does not critically affect the performance of the antennas due to the small distances they are projected to work on.

Furthermore, by analysing the radiation waves on the different coordinate-plane views, it is noticeable that, after the phase shift produced by the RA, a plane wave is reflected perpendicularly to it, meaning, in the z direction.

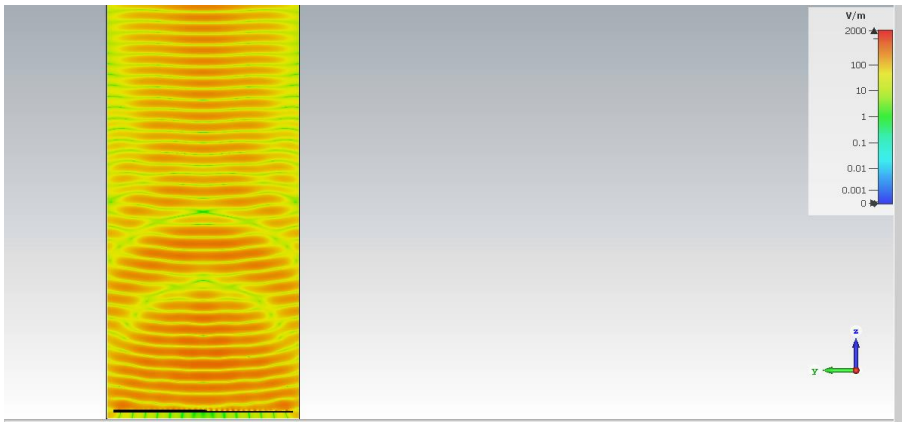

Figure 48 - YZ plane cut at x=o, the centre of the RA

On a different perspective, at z=1.5 m, the distance where the 30 cm RA will be positioned at, according to the problem geometry, Figure 14, the reflected wave arrives to that distance almost centred to the RA.

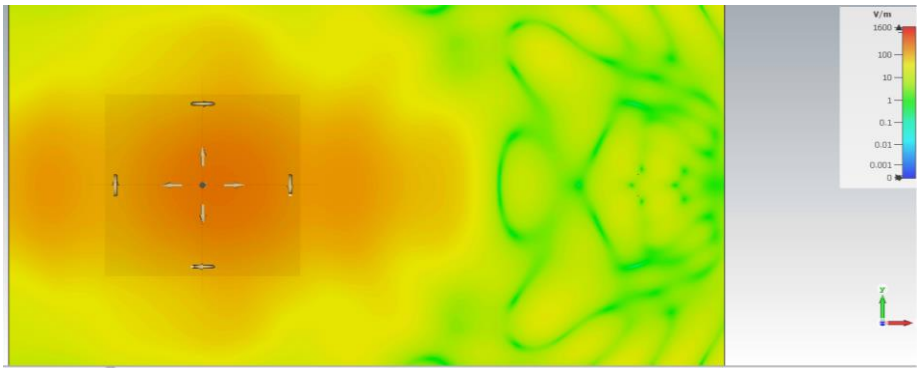

Figure 49 - YX plane cut at z = 1.5 m, position of the second RA

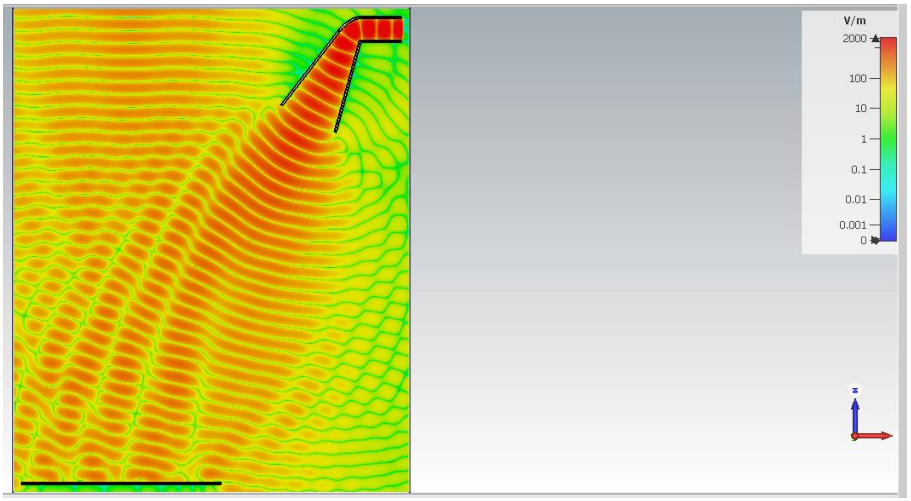

Figure 50 - XZ plane cut at Y = 0, centre of the RA

After the horn antenna radiates towards the 10x10 cm RA, a plane wave results from the phase correction, with a vertical direction. On Figure 49, the maximum incidence of the plane wave is almost centred with the RA.

5.8.2. 30 cm Reflect Array

The study proceeds with the creation and simulation of the 30 cm RA. Due to its size the creation of this RA makes the CST file extremely heavy, which becomes a major problem for the simulation matter. The simulation takes longer, and, therefore, the horn feed cannot be included on it.

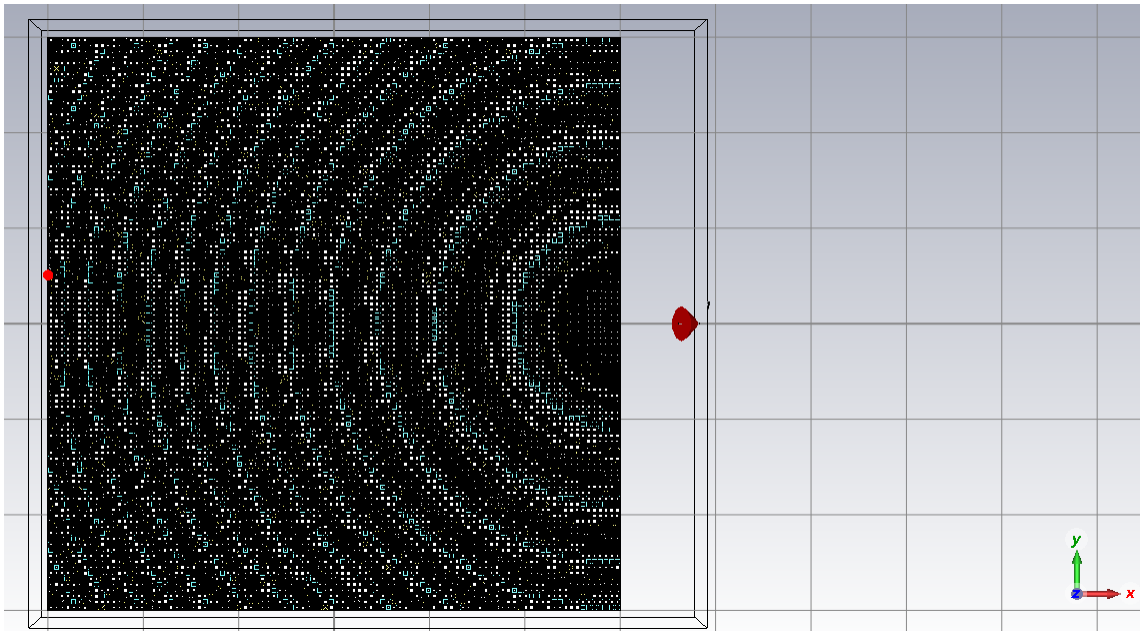

Figure 51 - 30 cm RA on CST

Like the 10 cm RA, a KH3D simulation is fundamental for comparisons and understanding how the RA, on the CST simulation, is behaving.

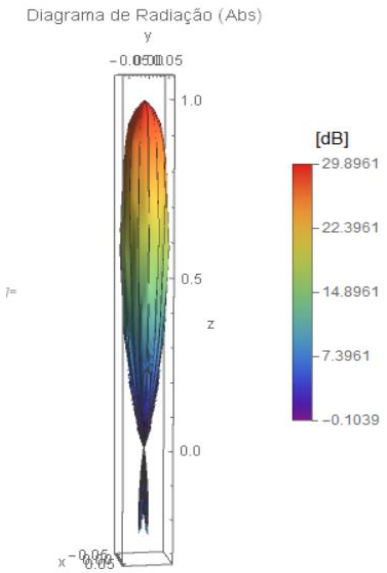

Figure 52 - 30 cm RA radiation pattern, calculated by KH3D

The same process is used to obtain the KH3D radiation pattern: a feed positioned at the desired point, radiating towards the 30 cm RA antenna, which then radiates it to the desired direction.

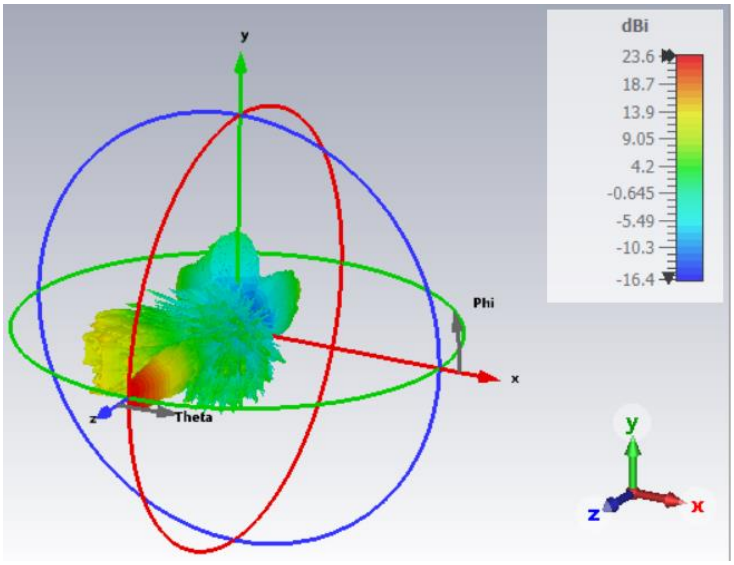

Figure 53 – far field results for the 30 cm x 30 cm RA at 24 GHz

On a first analysis, the radiation pattern presents unexpected losses of about 14 dBi, closed to the focusing direction, as seen in Figure 54 and Figure 55.

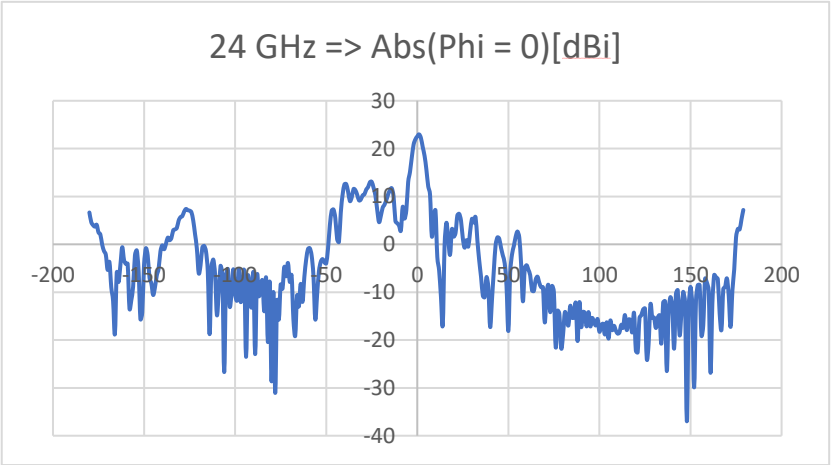

Figure 54 - Radiation pattern on the Phi = 0 plane

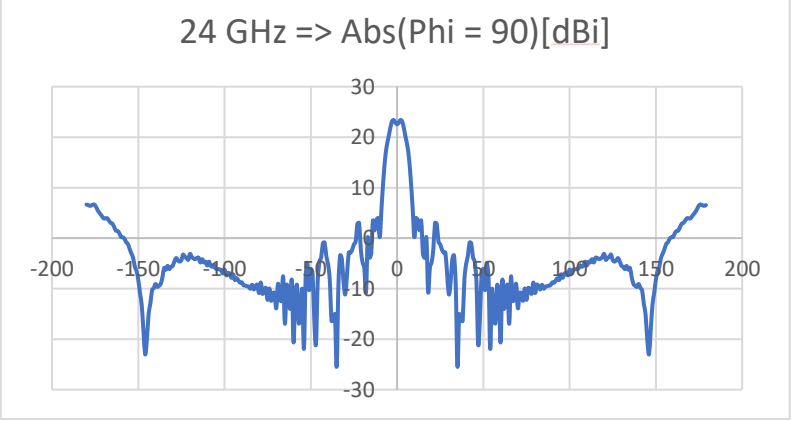

Figure 55 - Radiation pattern on the Phi = 90 plane

Despite the losses displayed in the previous figures, the results prove the concept of reflecting the Gaussian beam. Nevertheless, it is important to understand its behaviour for other frequencies. The different radiation patterns show that, as the frequency increases, the beam definition becomes better and the losses decrease.

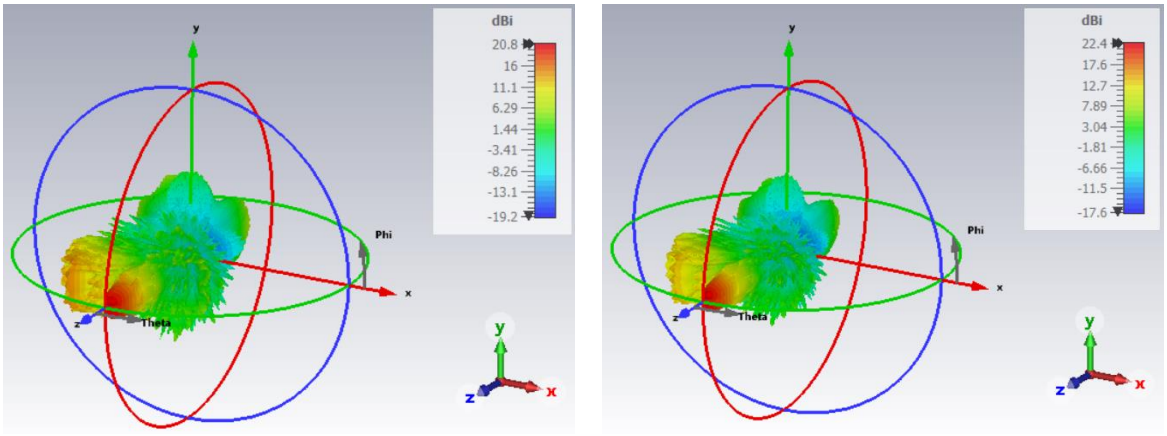

Figure 56 -radiation patterns for frequencies bellow 24 GHz: 23 GHz (left) and 23.5 GHz (right)

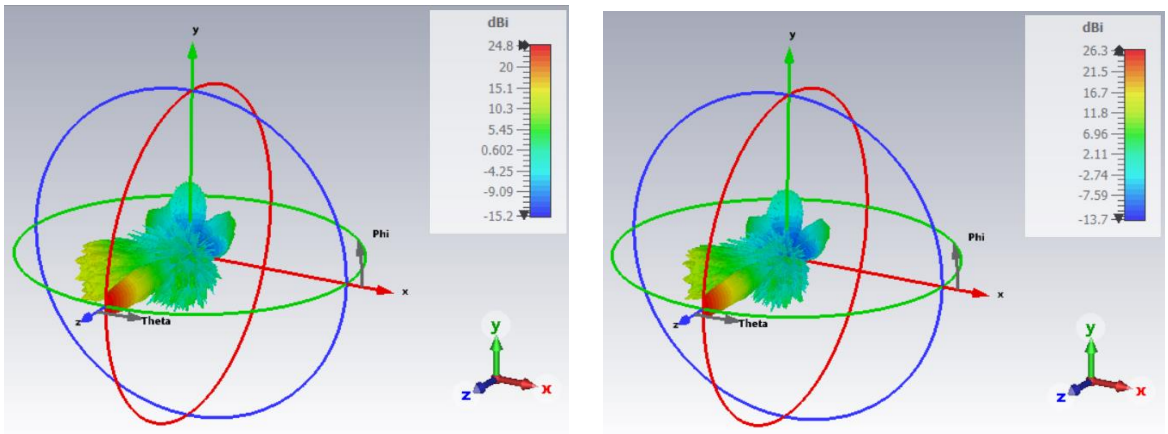

Figure 57 - radiation patterns for frequencies above 24 GHz: 24.5 GHz (left) and 25 GHz (right)

6. Experimental Results

For the experimental simulations, the two RAs must be fabricated, by printing the unit cell's distribution on a metallic surface, called substrate. For this process, the unneeded parts of the material should be removed, applying a procedure called Chemical Etching. With this process, a chemical is used to draw all the desired patterns and remove the unnecessary material parts, with as much precision as possible.

In a more detailed way, after choosing the material to be used, in this case the substrate *Rogers RT5880,* the metal goes through a pre-cleaning process to remove any debris that it may have, ensuring the surface is perfectly cleaned of any impurities that could cause underperformance of the antenna.

A mask is created for the antenna, where the cells' design is painted in black, to create a negative view of the antenna. After being printed, it is then laminated to the copper substrate. This will allow, in further procedure moments, to act as a shielding mask during the photo-exposure process.

The next step is to insert the surface, with the antenna mask stick to it, into the ultraviolet-light exposure (the proper surface should face the light). The photo-resit exposed to the ultraviolet light becomes hard and dark blue in colour, while unexposed photo-resist remains light blue and dissolves in the developer solution (Sodium Carbonate)

The final step is to chemically etche the developed surface with Ferric Chloride FeCl3 solution. The copper parts except underneath the hardened photo resist dissolve in FeCl3. The etched substrate is rinsed in running water to remove any etchant and then dried. The hardened photo resist is removed using Sodium Hydroxide [35].

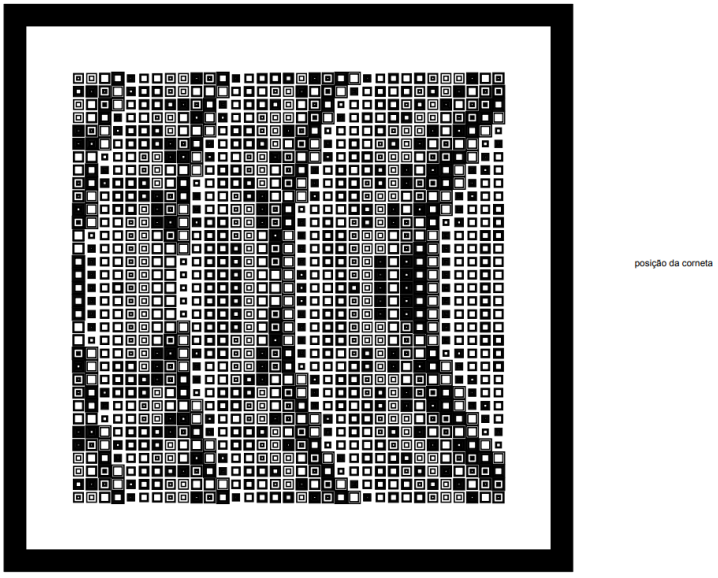

Figure 58 – 10 cm RA mask

Even though the lens mask is completed and printed on the metallic surface, it is still needed a structure to support the whole system: a base to stick the lens on it, and a look-a-like tower structure to support the horn antenna and position it at the desired height and angle, Figure 59 and.

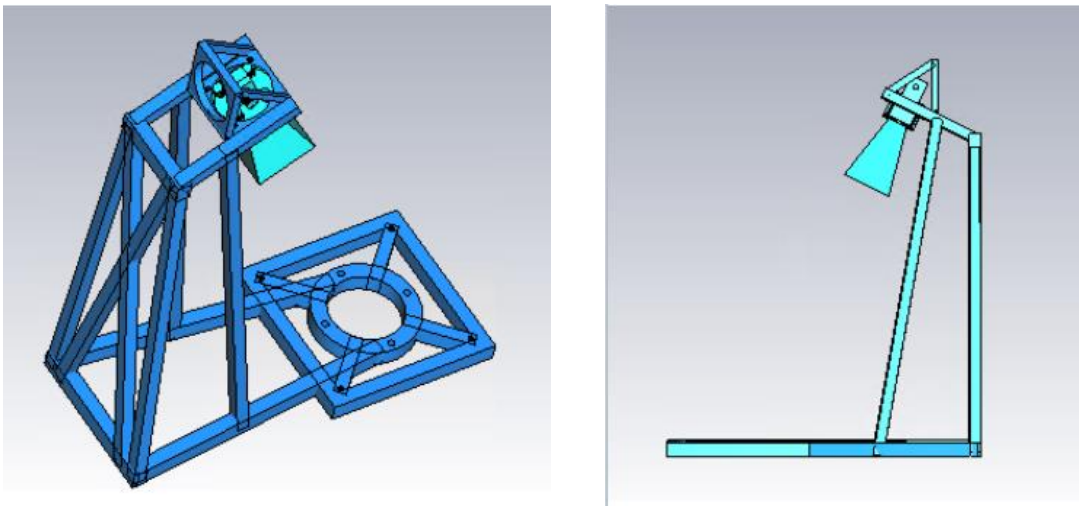

Figure 59 - 10 cm RA structure to support the smaller RA together with the horn antenna

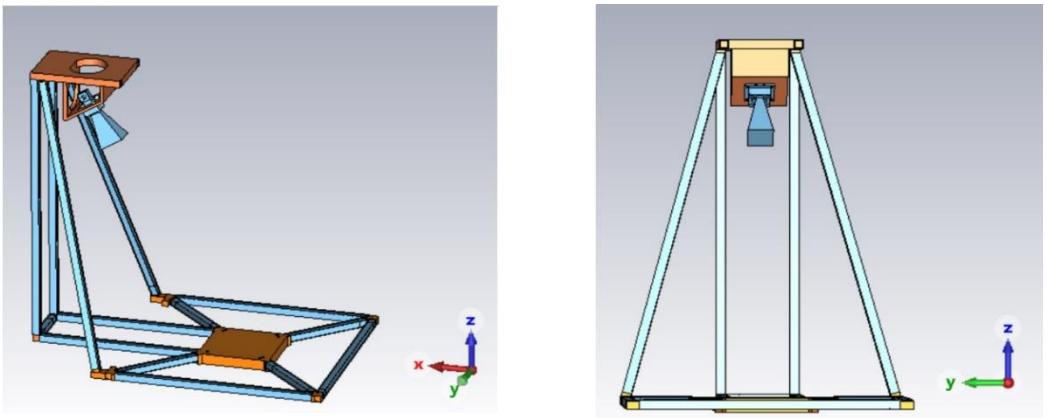

Figure 60 - 30 cm RA structure to support the larger RA together with the horn antenna

6.1. Experimental Results environment

The experimental simulations, after the construction of the lens and the structure, is performed on an environment that simulates the outer space, using the micro-wave anechoic chamber at Instituto Superior Técnico.

At this chamber, it is possible to simulate the system, avoiding reflection phenomenon that could be generated by walls, celling, or floor. The whole room is covered by an absorbing material, in pyramid shapes, to absorb the radiation.

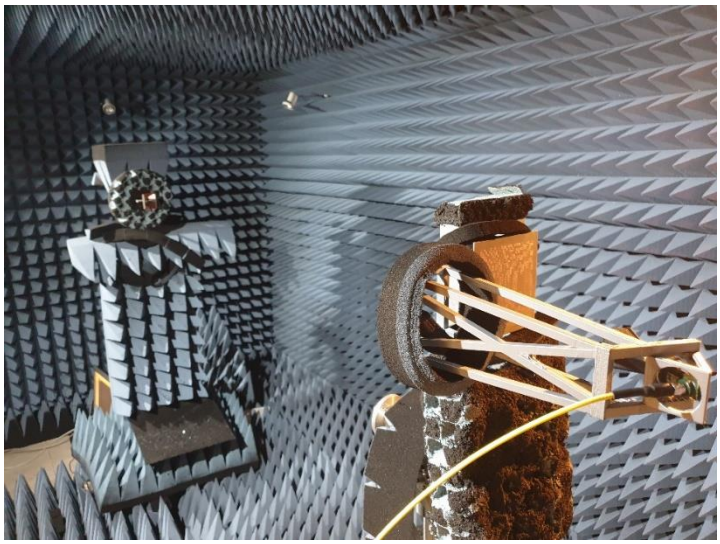

Figure 61 – 10 cm Antenna prototype simulating at the anechoic chamber at Instituto Superior Técnico

6.2. Reflect arrays experimental Results

The following and final step of the simulations process is to perform experiments, first with the reflect arrays individually, then with the whole system of the RA combined. The idea is to study the factual behaviour of each reflect array in terms of co-polarization and cross-polarization, as well as the directivity given the maximum gain obtained. Then the comparison between CST results and experimental results can give a good comparison between how is the RA behaving and what is the expected results.

Only after this individual analysis, the system can be truly simulated and reviewed, to understand if its energy transfer efficiency is an enough result to prove this study to be a good alternative for WPT.

6.2.1. 10 cm Reflect array

For the analysis of the following results, it is crucial to analyse the co-polarization graphic, Figure 62, which defines the desired polarization and direction, alongside with the signal strength, all together with the cross-polarization graphic, Figure 63 (strength of the noise, and polarization and direction orthogonal to the desired ones). [35]

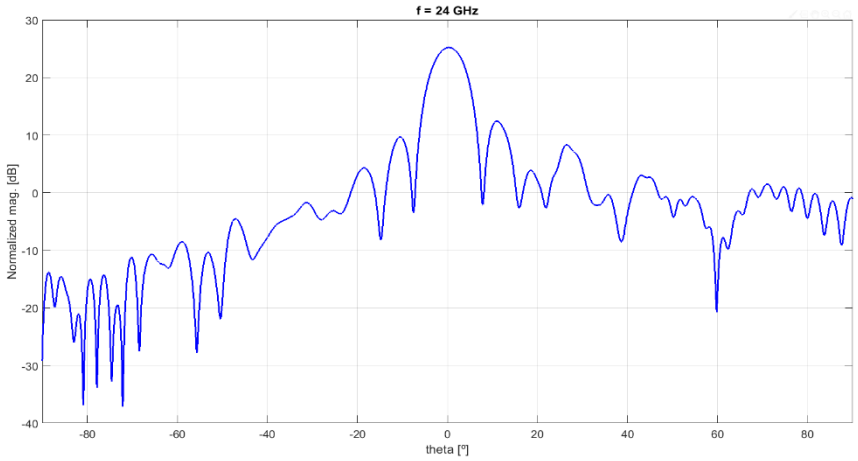

Figure 62 - Co-polarization radiation pattern at 24 GHz, obtained from the experimental simulation. Normalized at the peak of the directivity obtained on the CST software (25.2 dB)

The simulation presents a co-polarization radiation pattern, Figure 62, with the main beam almost centred at theta = 0 degrees, with the same deviation proportionality as on the CST (1 degree) and, therefore, a non-symmetrical graphic representation of the side lobes.

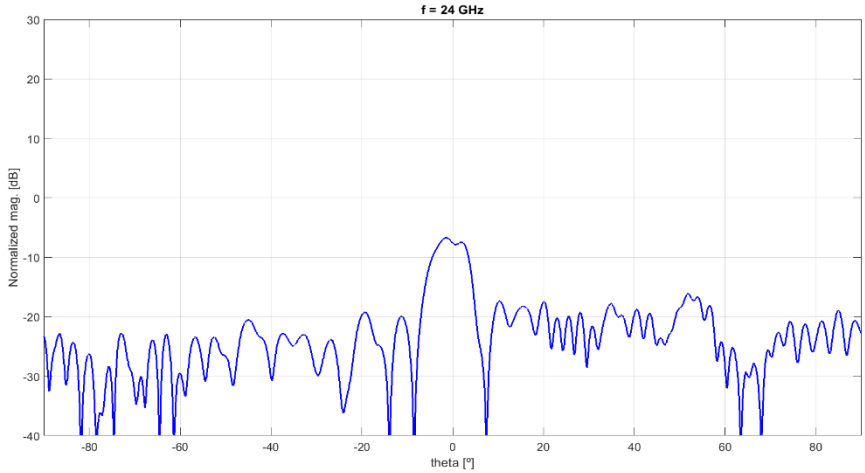

Figure 63 - Cross-polarization radiation pattern at 24 GHz, obtained from the experimental simulation.

With the obtained results for the horn antenna, it is possible to define the experimental gain and, therefore, make a crucial comparison with the CST results.

When comparing the co-polarization simulation with the results from the CST, not only the lobes (main and side) present a similar behaviour, but also the difference between both gains is minimal.

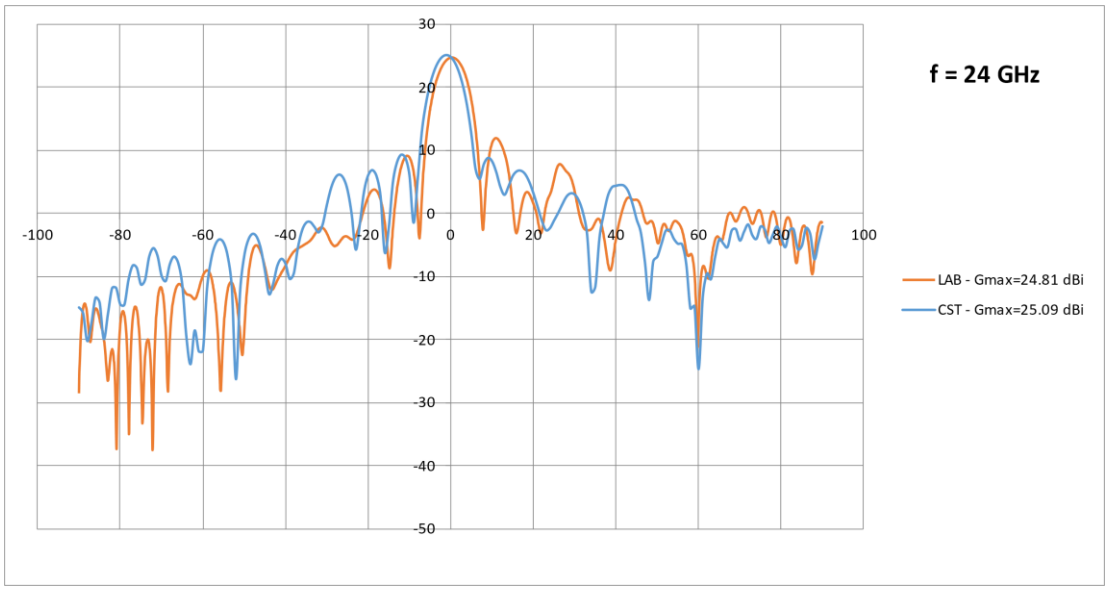

Figure 64 - Comparison between CST and experimental results at 24 GHz, with maximum gain information

Besides the comparison at 24 GHz, other simulations are performed for four different frequencies, and compared to understand if the used frequency (24 GHz) is actually the one that presents the most accurate results.

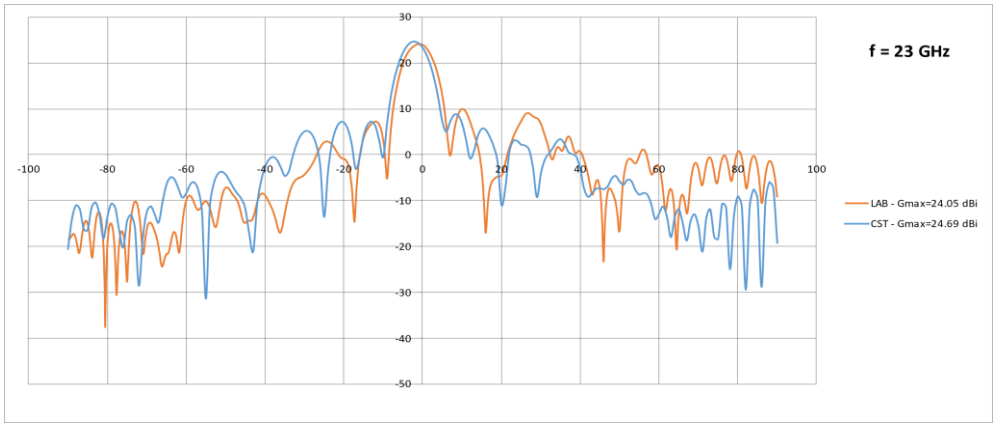

Figure 65 - Comparison between CST and experimental results at 23 GHz, with maximum gain information

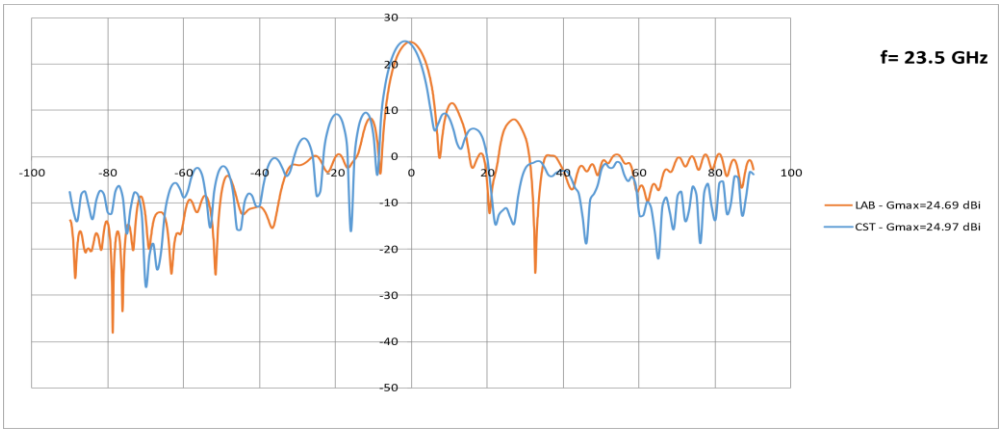

Figure 66 - Comparison between CST and experimental results at 23.5 GHz, with maximum gain information

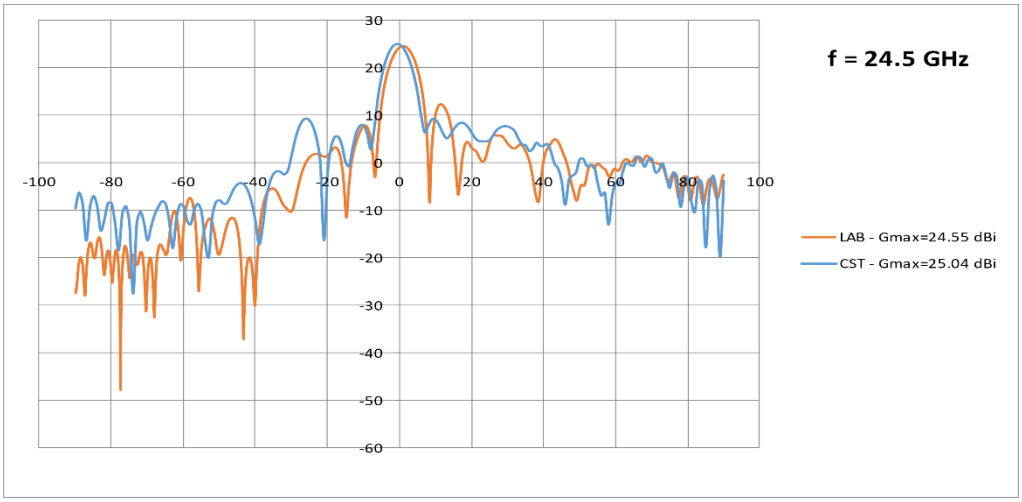

Figure 67 - Comparison between CST and experimental results at 24.5 GHz, with maximum gain information

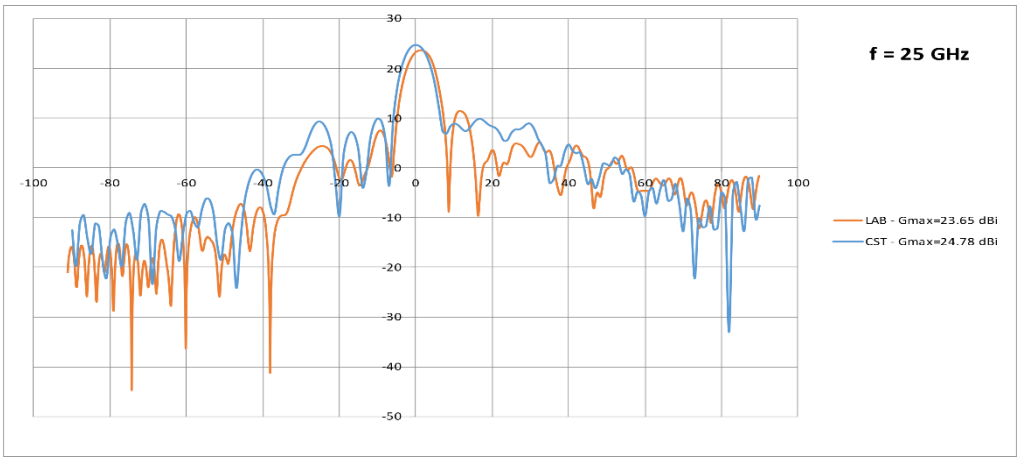

Figure 68 - Comparison between CST and experimental results at 25 GHz, with maximum gain information

After analysing all the data for all the five frequencies, it can be summarized on a table that directly indicates the performance/behaviour on each frequency.

Frequencies (GHz)	Max Gain – CST [dB]	Max Gain – LAB [dB]	Gain difference [dB]
23	24.69	24.05	0.64
23.5	24.97	24.69	0.28
24	**25.09**	**24.81**	**0.28**
24.5	25.04	24.55	0.49
25	24.78	23.65	1.13

Table 4 - Comparison, for different frequencies, of the Gain obtained through CST and through experimental results

At 24 GHz, not only the obtained maximum gain on the CST is the best, but also the obtained maximum gain through experimental results. Furthermore, the actual difference between these two gains is the lowest, which confirms the 24 GHz frequency to be the best one in terms of performance.

6.2.2 30 cm Reflect array

After the first RA's results are obtained and analysed, the same process runs through the 30 cm RA.

Due to its large file size, it was not possible to simulate the polarizations, nor to obtain the gain. Therefore, the study made for this reflect array is only based on the experimental results.

The behaviour of the 30 cm RA shows a slight deviation in frequency, where at 24 GHz is sopose to obtain the highest maximum gain.

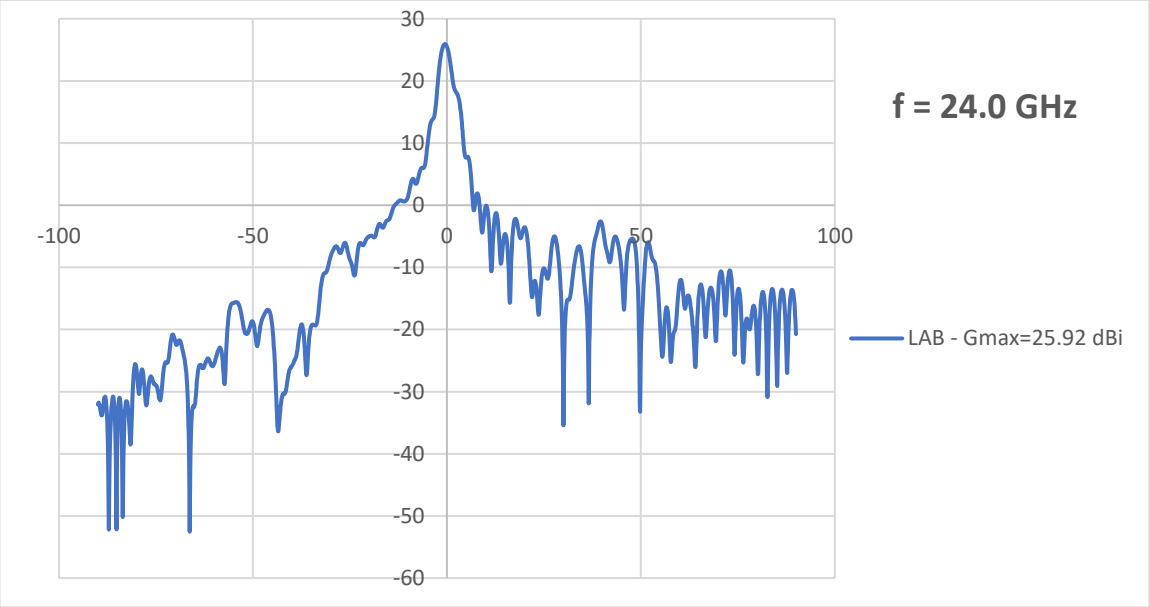

Figure 69 – Radiation pattern calculated from the experimental results at 24 GHz, with maximum gain information

The resulting radiation pattern has a well-defined maximum at zero degrees, with an obtained maximum gain of 25.92 dB, a good result regarding the one obtained for the same frequency for the 10 cm RA.

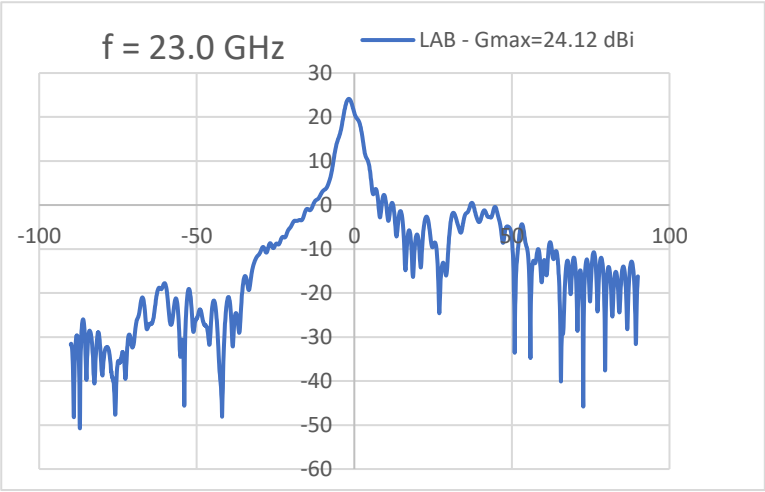

Figure 70 Radiation pattern calculated from the experimental results at 23 GHz, with maximum gain information

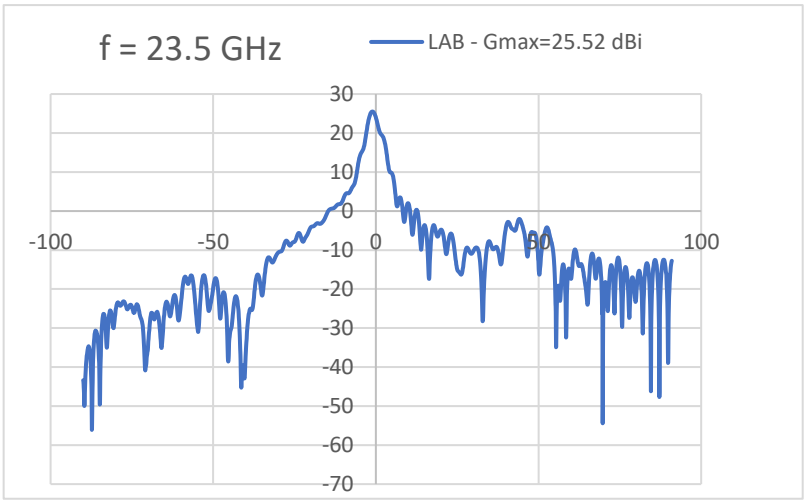

Figure 71 - Radiation pattern calculated from the experimental results at 23.5 GHz, with maximum gain information

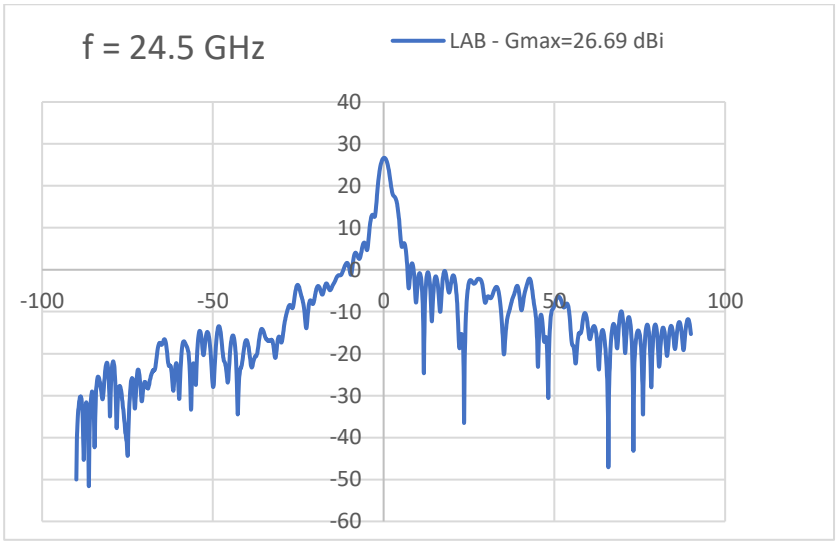

Figure 72 - Radiation pattern calculated from the experimental results at 24.5 GHz, with maximum gain information

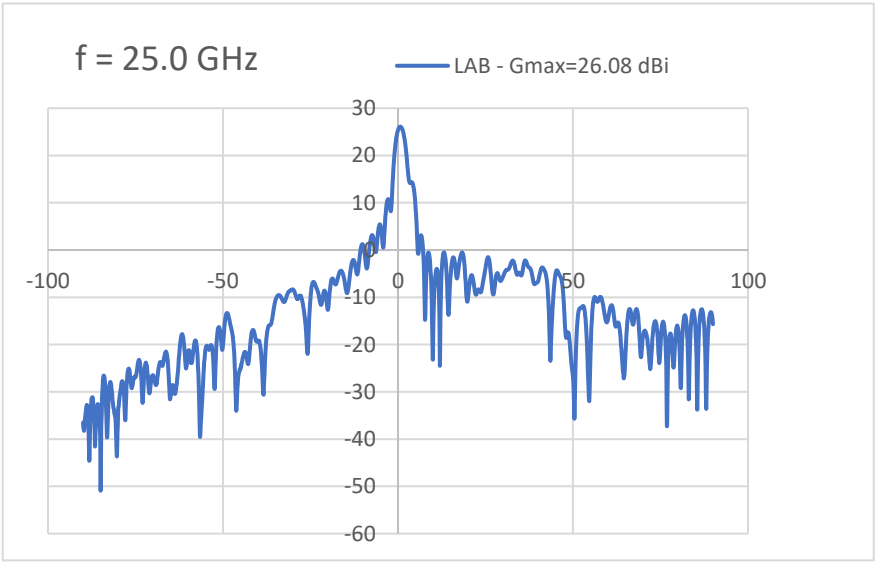

Figure 73 - Radiation pattern calculated from the experimental results at 25 GHz, with maximum gain information

Frequencies (GHz)	Maximum Gain – LAB (dB)
23.0	24.12
23.5	25.52
24.0	**25.92**
24.5	26.69
25.0	26.08

Table 5 - Maximum Gain results obtained in the LAB for different frequencies

From the analysis made to create Table 5, for frequencies higher than 24 GHz, the maximum gain grows even more, proving the frequency deviation mentioned before.

6.2.3 Reflection Results of the whole system

For the remaining experimental tests, it is first important to notice that they won't be performed from an end-to-end point of view, since the laboratory does not have DC-RF and RF-DC convertion blocks. Therefore, the measurments are performed between the horn's ports.

The goal is to measure the total S21 of the system, to analyse the insertion losses.

In a perfect scenario, the insertion loss of the whole system would be 0 dB, meaning 100% of efficiency between horns. This efficiency will never achieve such result due to all the losses it has throughout all system components. Those losses include reflection at the port 1 entry; horn antenna losses; spill-over from illuminating the 30 cm RA; larger RA radiation efficiency, due to phase errors; Gaussian beam non-perfect definition, spill-over from illuminating the 10 cm RA; smaller RA radiation efficiency and Rx horn insertion losses.

For those reasons, it is important to proceed with further simulations to understand if the behaviour of each component is the expected or how it is impacting the final result.

The S21 results are obtained for different depths (mm), meaning, for different distances between two components. Eventhough the system was designed to work at a distance of 1.5 m, the laboratorial set-up had its limitations, allowing to go down only o 1544 mm for the first three measurements, excluding the ones for the total system. Two different distances are considered: 1544 mm, the minimum obtained for all measurments, and 1600 mm, the medium value for depth.

The first performed measurment is the transmission between two standard horn antennas. This gives us the S21 used as a reference, S21_REF.

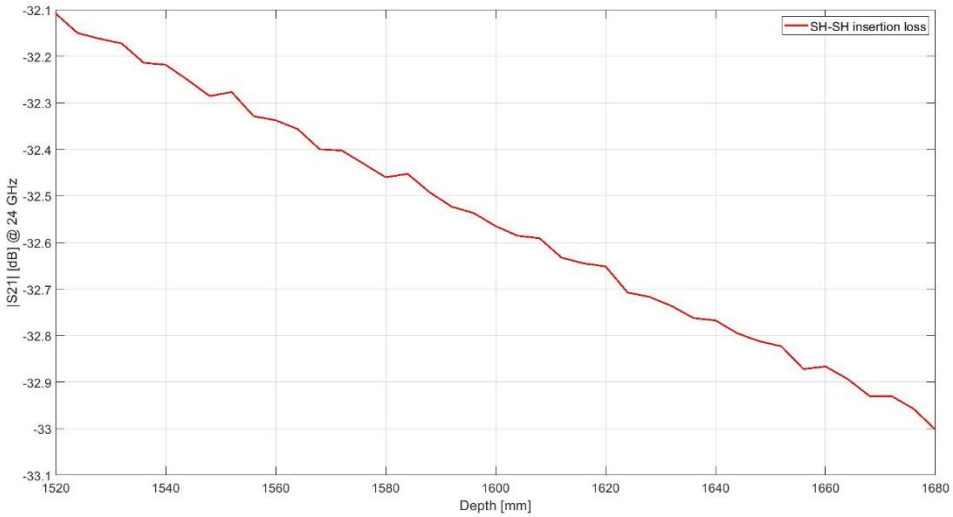

Figure 74 - reference insertion loss, S21_REF, between two standard horn antennas

At 1544 mm, the S21_REF is -32.25 dB, and -32.56 dB for 1600 mm. Therefore, as depth reduces towards the 1500 mm, so does the insertion losses are less.

The second performed measurement is between the 10 cm RA and a standard horn antenna, S21_RA10.

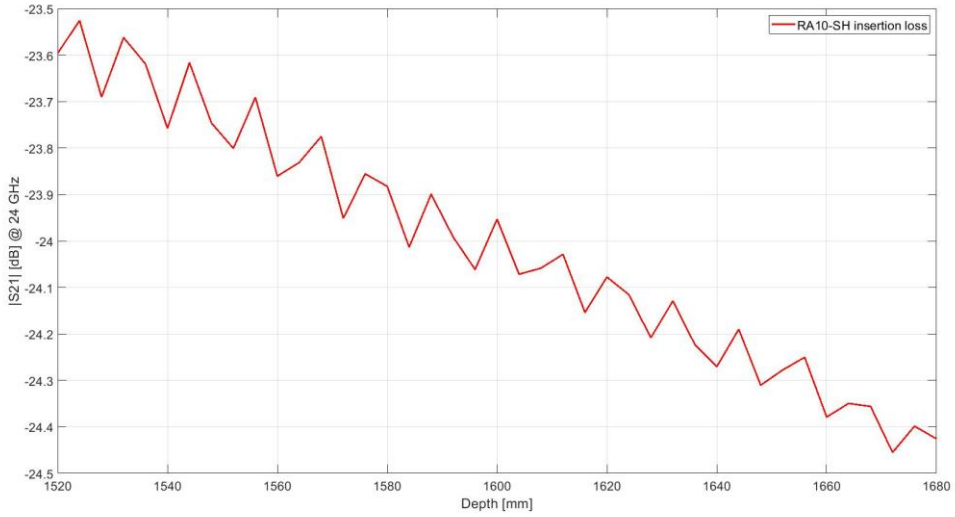

Figure 75 - insertion loss between a standard horn antenna and the 10 cm RA, S21_RA10

At 1600 mm, the S21_RA10 is -23.95 dB, while at 1600 mm is -23.62 dB proving, once again, the losses reduction with the depth.

The same process must be performed between a standard horn antenna and the 30 cm RA, S21_RA30. For this case, it is expected that the S21_RA30 gets better results than the S21_RA10, since the RA area is bigger, avoiding more insertion losses than the 10 cm RA.

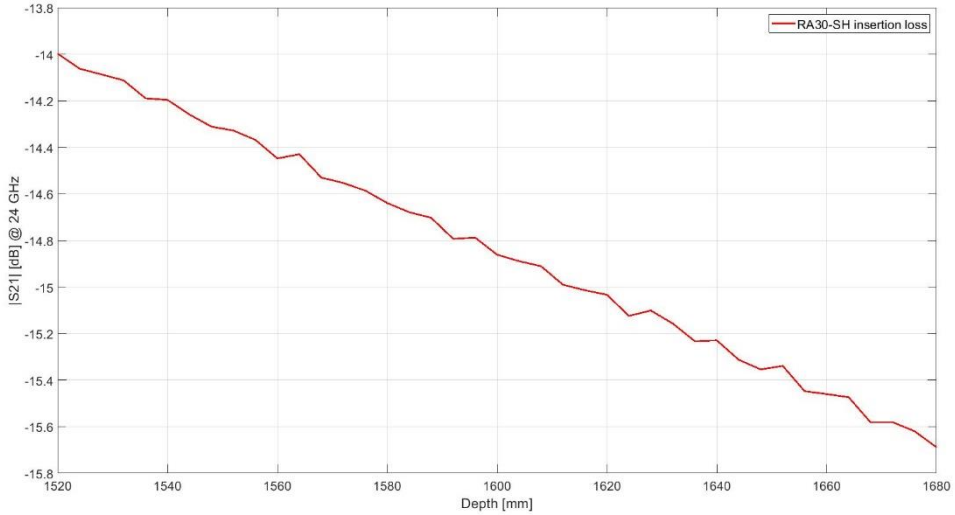

Figure 76 - insertion loss between a standard horn antenna and the 30 cm RA, S21_RA30

Has expected, the results for the S21_RA30 are better, more specifically of -14.26 dB and -14.86 dB, for 1544 mm and 1600 mm respectively.

The process concludes with the measurements of the whole system, with distances between 1420 and 1540: from port 1 to Tx horn antenna, radiating a spherical wave towards the 30 cm RA, which, after phase correction, radiates a Gaussian beam towards the 10 cm RA, which radiates again a spherical wave towards the Rx horn antenna. This will give the S21_TOTAL. The results are present on Figure 77.

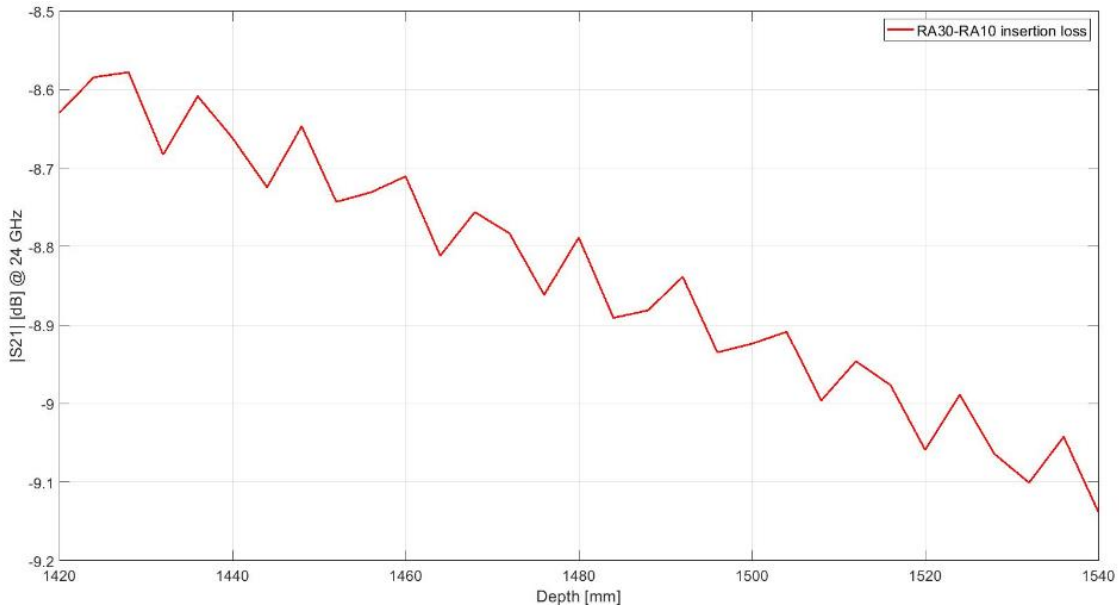

Figure 77- insertion loss between the 30 cm RA and the 10 cm RA, S21_TOTAL

Once again, the S21_TOTAL has even better results. At 1500 mm the insertion loss obtained is of -8.924 dB, representing an efficiency of 12.81%. Other results, specifically for 24.5 GHz and 24.03 GHz are mentioned: the first one since it is at this frequency that the maximum gain was obtained; the second one where it is obtained the highest efficiency,

S21_TOT	1500 mm	Efficiency
24 GHz	-8.924 dB	12.81%
24.5 GHz	-9.648 dB	10.84%
24.03 GHz	-8.87 dB	12.97%

Table 6 - dB comparison of the s21 coefficient for different frequencies. Includes also the transmission efficiency

These results prove to be a better achievement than the one obtained with a Quasioptical Dielectric Lens System [19], where the obtained efficiency was of 4%. Nevertheless, an efficiency of 11.74% shows that the system may have its limitations for this type of context approach.

7. Conclusions and Future Work

7.1. Conclusions

The main objective of this thesis is to study the Wireless Power Transfer between two different CubeSat, launched to space in a batch, considering the near-field distances, in this case, 1.5 m. The frequency bandwidth in use is in the range of 20-30 GHz, more specifically, at 24 GHz. This frequency choice is based on the fact the antennas must have higher gains to sustain a stable focus direction of the beam signal and avoid as much spill-over as possible. For the purpose, Gaussian beams solution is studied to improve the power transfer efficiency.

Since the CubeSat are low-cost launches, the antennas must be flat to ensure the minimum space cover possible, and then be deployed when on space.

The main idea is then to study two different reflect arrays, with different sizes (1U and 3U) and their capability of radiating the radiated beam to the position where the other CubeSat stands.

This study performs by proposing two RAs, one of 10x10 cm, and the other of 30x30 cm, that are populated with unit cells to phase shift the circular reflected beam to the desired direction, now as a Gaussian Beam with a planar phase.

The two lenses are simulated, after studying their behaviour on a program called KH3D, using the software CST-MWS. With this program, the lenses are populated with the previously mentioned unit cells, and then, with the aid of a horn antenna operating at a maximum directivity of 16 dB, and simulated at far-field level, to understand the behaviour of the main and side lobes, as well as directivity and beam direction. The horn antenna is positioned at a focal point, different for each lens considering the size of the CubeSat and tilted so they hit the RAs right at their central point.

The 10x10 cm lens proved to be efficient in terms of performance, with a maximum gain at 25.09 and a total efficiency of 94.08%, and a slight deviation of the main beam direction (1 degree). The 30x30 cm lens also proves to fulfil its goal, even though the best performance is deviated in the frequency, for ones higher than 24 GHz.

After the simulations on the CST-MWS are completed, a mask for each lens is then created, to imprint their pattern on a metallic surface, substrate, in this case the Rogers RT5880 (lossy). In parallel with this process, the structures that sustain the lenses and the horn antenna at fixed positions are designed and manufactured. When the whole system is completed, it is time to proceed to the laboratorial exercises, where further simulations, now with both prototypes, are performed.

The 10x10 cm lens performance proves, once again, to be of high standard. The radiation pattern is similar to the obtained via CST and the obtained maximum gain is of 24.81, leading to a difference of 0.28 dB from the CST. When comparing to the same results for other four and range close frequencies, not only the obtained gains are higher but also the difference hits its lowest value. For the 30 cm RA, even though the results are satisfactory, with a well-defined main lobe and a reasonable maximum gain, they cannot be compared to the CST simulations, since due to the file size it was not possible to obtain the maximum gain for it.

With both lenses studied individually, the system could then be simulated to understand how the insertion loss, S21, was working through the depth. At 1500 mm, the obtained insertion loss, for 24 GHz is -8.924 dB; -9.648 dB for 24.5 GHz and -8.87 dB for 24.03 GHz, leading to an efficiency of 12.81%, 10.84% and 12.97%, respectively. These results prove to be an improvement, when compared to other solutions presented in previous studies. However, from a usability point of view, it still has its limitations for satellites use purposes.

7.2. Future Work

The 10x10 cm RA lens, despite eventual human errors, proves to perform the needed and desired behaviour to successfully wireless power transfer on a small distance of 1.5 m.

On the CST simulation results, the lens deviated the beam in one degree. It would be important to understand the impact of unit cells' design errors on the aperture's performance. Furthermore, the composition of the unit cells throughout the lens area was not symmetrical due to human error, even though due to symmetries applied on the model it ended up behaving that way. Nevertheless, this occurrence may have had impact on the lenses performance, both in CST and lab.

As mentioned before, the 30x30 cm RA was troublesome, due to its extremely large file size. The resultant CST radiation pattern was "broken". Furthermore, it was deviated in the frequency, meaning its best result could not be used for the desired frequency.

Alongside with the large size of the CST file for simulation purposes, the printing of the 30 cm RA mask also proved to become a major problem: its size highly affected the creation of an image of the mask properly defined to print it on the metallic surface. This made the process of creating the prototype even harder and it may have affected the final result in terms of printed unit cells.

Another way of trying to improve the efficiency results would be to increase the reflect arrays area, to decrease the losses by spillover. This reduces the aperture efficiency, so a middle term should be achieved.

In sum, the main subject of improvements is the reduction of energy losses by spill over.

References

[1] H. Helvajian and S. W. Janson, Small Satellites: Past, Present, and Future.

[2] M. N. Sweeting, “"Modern Small Satellites - Changing the Economics of Space"," *Proceedings of the IEEE,* vol. 106, no. 3, 2018.

[3] S. W. Janson, “25 Years of Small Satellites,” *SSC11-III-1.*

[4] A. H. Abdelrahman, A. Z. Elsherbeni and F. Yang, “Transmission Phase Limit of Multilayer Frequency-Selective Surfaces for Transmitarray Designs,” *IEEE Transactions on Antennas and Propagation,* vol. 62, Februrary 2014.

[5] “Phased Array,” [Online]. Available: https://en.wikipedia.org/wiki/Phased_array. [Accessed 03 june 2020].

[6] N. Parinaz, S. A. Matos, J. R. Costa and C. A. Fernandes, “Phase-Delay Versus Phase-Rotation Cells for Circular Polarization Transmit Arrays - Application to Satellite Ka-Band Beam Steering,” *Antennas and Propagation,* vol. 66, no. 3, pp. 1236-1247, 2018.

[7] E. B. Lima, S. A. Matos, J. R. Costa, C. A. Fernandes and N. J. G. Fonseca, “Circular Polarization Wide-Angle Beam Steering at Ka-Band by In-Plane Translation of a Plate Lens Antenna,” *Antennas and Propagation,* vol. 63, no. 12, pp. 5443-5455, december 2015.

[8] “Guide to the Nuclear Wall Chart,” [Online]. Available: https://www2.lbl.gov/abc/wallchart/chapters/13/10.html. [Accessed 12 July 2020]. [Accessed 12 july 2020].

[9] “Scielo,” 25 october 1999. [Online]. Available: https://www.scielo.br/scielo.php?script=sci_arttext&pid=S0102-261X1999000200005. [Accessed 12 july 2020].

[10] S. Sasaki and K. Tanaka, “Wireless Power Transmission Technologies for Solar Power Satellite,” in *2011 IEEE MTT-S International Microwave Workshop Series on Innovative Wireless Power Transmission: Technologies, Systems, and Applications*, Kyoto, Japan, 2011.

[11] “Development of 24 GHz Rectennas for Fixed Wireless Access,” in *2011 XXXth URSI General Assembly and Scientific Symposium*, Istanbul, Turkey, 2011.

[12] C. Bergsrud and J. Straub, “A space-to-space microwave wireless power transmission experiential mission using small satellites,” pp. 193-203, 02 july 2014.

[13] D. R. Smith, V. R. Gowda, O. Yurduseven, S. Larouche, G. Lipworth, Y. Urzhumov and M. S. Reynolds, “An Analysis of Beamed Wireless Power Transfer in the Fresnel Zone using a Dynamic, Metasurface Aperture,” *Journal of Applied Physics,* 2017.

[14] A. Z. Elsherbeni, P. Nayeri and F. Yang, “Reflectarray Antennas for Space Applications,” in *IEEE International Conference on Ultra-Wideband*, Syracuse, NY, USA, 2012.

[15] V. R. Gowda, O. Yurduseven, G. Lipworth, T. Zupan, M. S. Reynolds and D. R. Smith, “Wireless Power Transfer in the Radiative Near Field,” *IEEEE SS PROPAGATION LETTERS,* vol. 15, pp. 1865-1868, 2016.

[16] S. PAKOVIC, S. ZHOU, D. GONZÁLEZ-OVEJERO, S. CONCETTO PAVONE, A. GRBIC e M. ETTORRE, “Bessel–Gauss Beam Launchers for Wireless,” *IEEE Open Journal of Antennas and Propagation,* vol. 2, pp. 654-663, 2021.

[17] A. Gonzalez, Y. Uzawa, Y. Fujii, K. Kaneko e K. Kuroiwa, “A horn-to-horn power transmission system at terahertz frequencies,” *IEEE Transactions on Terahertz Science and Technology,* Vols. %1 de %21, 2, pp. 416-424, 2011.

[18] R. Pereira e N. Carvalho, “Quasioptics for Increasing the Beam Efficiency of Wireless Power Transfer Systems,” Research Square, 2022.

[19] R. A. M. Pereira e N. B. Carvalho, “Quasioptical Dieletric Lens System for WPT solutions,” *2022 Wireless Power Week,* pp. 190-194, 2022.

[20] Y. Rahmat-Samii, “Large Antennas in Space: Concepts, Options and Challenges,” 2001.

[21] S. H. Hsu, C. Han, J. Huang and K. Chang, “An Offset Linear-Array-Fed Ku/Ka Dual-Band Reflectarray for Planet Cloud/Percipitation Radar,” *Antennas and Propagation,* vol. 55, pp. 3114-3122, 2007.

[22] T. Chaloun, C. Hillerband, C. Waldschmidt and W. Menzel, “Active Transmitarray Submodule for K/Ka Band Satcom Applications,” in *Microwave COnference (GeMic)*, Nuremberg, Germany, 2015.

[23] S. A. Matos, E. B. Lima, J. S. Silva, J. R. Costa, C. A. Fernandes, N. J. G. Fonseca and R. Mosig, “High Gain Dual-Band Beam-Steering Transmit Array for Satcom Terminals at Ka-Band,” *IEEE Transactions on antennas and propagation,* vol. 65, no. 7, pp. 3528-3539, july 2017.

[24] R. E. Hodges, D. J. Hoppe, M. J. Radway and N. E. Chahat, “Novel Deployable Reflectarray Antennas for CubeSat Communications,” 2015.

[25] R. E. Hodges, M. J. Radway, A. Toorian, D. J. Hoppe, B. Shah and A. E. Kalman, “ISARA - Integrated Solar Array and Reflectarray CubeSat Deployable Ka-Band Antenna,” pp. 2141-2142, 2015.

[26] J. G. Nicholls and S. V. Hum, “Full-Space Electronic Beam-Steering Transmitarray with Integrated Leaky-Wave Feed,” *IEEE TRANSACTIONS ON ANTENNAS AND PROPAGATION,* vol. 64, no. 8, pp. 3410-3422, august 2016.

[27] “Edmund Optics,” Edmund Optics, [Online]. Available: https://www.edmundoptics.com/knowledge-center/application-notes/lasers/gaussian-beam-propagation/. [Accessed 13 august 2020].

[28] C. A. Balanis, Antenna theory analysis and design, third ed., New Jersey: John Wiley & Sons, Inc, 2005.

[29] “L. Freznel, "electronic design",” 08 june 2012. [Online]. Available: https://www.electronicdesign.com/markets/energy/article/21801976/whats-the-difference-between-em-near-field-and-far-field. [Accessed 07 september 2020].

[30] J. R. Kopacz, R. Herschitz and J. Roney, “Small satellites an overview and assessment,” vol. 107, pp. 93-105, 2020.

[31] “TICRA,” [Online]. Available: https://www.ticra.com/rf-testing-of-ka-band-reflectarray-antenna-for-cubesat/. [Acedido em 09 september 2022].

[32] C. A. C. Fernandes, KH3D_near User's manual Version 0.2h, 2018.

[33] D. S. D. GmbH, CST Studio Suite - Getting Started, 2019.

[34] M. S. Palhade e S. P. Yawale, “Desing and Photo-Lithographic Fabrication of Microstrip Patch Antenna,” *International Journal of Science and Research (IJSR),* 2013.

[35] “alen space,” [Online]. Available: https://alen.space/basic-guide-nanosatellites/. [Accessed 24 april 2020].

[36] “CubeSat Design Specifications (CDS) Rev. 13,” 2014.

[37] “Feeding Systems of Phased Array Antenna - Radartutorial,” [Online]. Available: https://www.radartutorial.eu/06.antennas/Feeding%20Systems.en.html. [Accessed 18 november 2020].

[38] J. Rumburg, “Nasa Headquarters,” 07 august 2017. [Online]. Available: https://www.nasa.gov/content/goddard/nasas-science-mission-directorate-cubesat-initiative. [Accessed 19 april 2020].

[39] S. V. Hum and J. Perruisseau-Carrier, “Reconfigurable Reflectarrays and Array Lens for Dynamic Antenna Beam Control: A Review,” vol. 62, no. 1, pp. 183-198, january 2014.

[40] M. Y. Ismail, A. Faizal, M. Inam and N. Misran, “Mathematical Models for Progressive Phase Distribution of Ku-Band Reflectarray Antennas,” vol. 7, no. 12, pp. 1055-1059, december 2013.

[41] “everithing RF,” 22 may 2018. [Online]. Available: https://www.everythingrf.com/community/what-are-near-field-and-far-field-regions-of-an-antenna. [Accessed 07 september 2020].

[42] R. A. M. Pereira, “Gaussian Beam Microwave Antennas in Quasi-Optical Systems for Wireless Power Transfer,” 20117.

[43] “RP - photonics,” [Online]. Available: https://www.rp-photonics.com/gaussian_beams.html. [Accessed 13 august 2020].

[44] “Wikipedia - Gaussian Beam,” 21 October 2022. [Online]. Available: https://en.wikipedia.org/wiki/Gaussian_beam.